

Topological classification for chiral symmetry with non-equal sublattices

J. X. Dai¹ and Y. X. Zhao^{1,*}

¹*Department of Physics and HK Institute of Quantum Science & Technology,
The University of Hong Kong, Pokfulam Road, Hong Kong, China*

Chiral symmetry on bipartite lattices with different numbers of A -sites and B -sites is exceptional in condensed matter, as it gives rise to zero-energy flat bands. Crystalline systems featuring chiral symmetry with non-equal sublattices include Lieb lattices, dice lattices, and particularly Moiré systems, where interaction converts the flat bands into fascinating many-body phases. In this work, we present a comprehensive classification theory for chiral symmetry with non-equal sublattices. First, we identify the classifying spaces as Stiefel manifolds and derive the topological classification table. Then, we extend the symmetry by taking \mathcal{PT} symmetry into account, and ultimately obtain three symmetry classes corresponding to complex, real, and quaternionic Stiefel manifolds, respectively. Finally, we apply our theory to clarify the topological invariant for \mathcal{PT} -invariant Moiré systems and construct physical models with Lieb and dice lattice structures to demonstrate our theory. Our work establishes the theoretical foundation of topological phases protected by chiral symmetries with non-equal sublattices.

Introduction Sublattice on bipartite lattices with non-equal sublattices is an exceptional symmetry in condensed matter. This symmetry concerns a bipartite lattice hosting different numbers of A -sites and B -sites for the two sublattices [1, 2] and anti-commutes with the Hamiltonian that only couples A -sites and B -sites. Such sublattice symmetry is referred to as chiral symmetry with non-equal sublattices (CSNES). Elementary examples include the Lieb lattices and dice lattices [3–11], where every unit cell comprises a single A -site and two B -sites, as illustrated by Fig. 1a.

A characteristic of CSNES is the presence of $|M - N|$ flat bands at zero energy, where M and N are A and B site numbers in a unit cell, respectively (see Fig. 1c and d). The flat bands resulting from CSNES have recently attracted significant interest in Moiré systems, such as twisted bilayer graphene, where fascinating quantum phases can be formed through interactions [1, 2, 12]. Additionally, the Fermi points feature Berry dipole charge, as recently revealed [13, 14].

Naturally, a fundamental question arises: How to derive the topological classifications for CSNES.

Conventionally, chiral symmetry is considered under the framework of the tenfold Altland-Zirnbauer symmetry classes (AZ classes) [15–19]. Various topological classifications for the tenfold AZ classes play a seminal role in the development of symmetry protected topological phases that have dominated modern condensed matter physics and beyond in recent years [20–25]. In applying the tenfold topological classifications to bipartite lattices, there is a presumption, i.e., in each unit cell the number of A -sites is equal to that of B -sites, as exemplified by the Su-Schrieffer-Heeger model in Fig. 1b. However, this presumption has been violated in the case of CSNES. Consequently, the chiral AZ classes always assume a gap at zero energy, which is inconsistent with the aforementioned zero-energy flat bands originating from CSNES.

This work is devoted to presenting a comprehensive

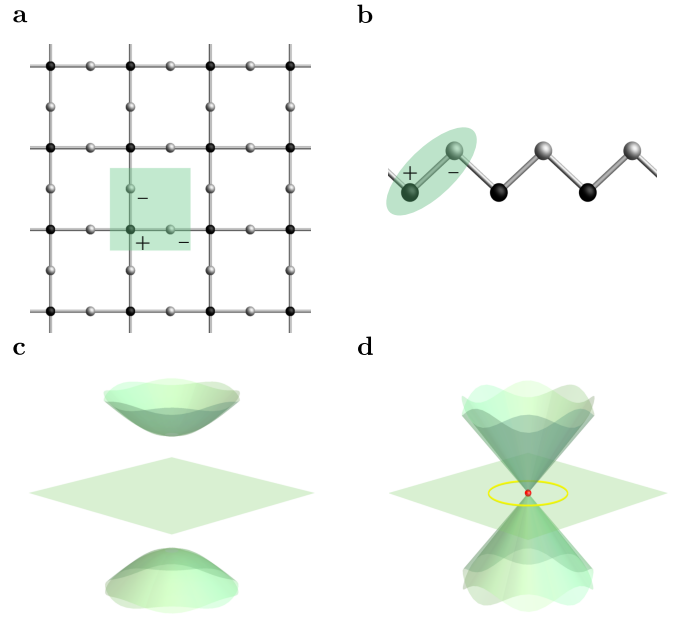


FIG. 1. **a** and **b** illustrate the Lieb lattice model and the Su-Schrieffer-Heeger model, respectively. Unit cells for them are marked by shadowed regions, where A -sites and B -sites are marked in black and grey and assigned signs \pm by the sublattice symmetry, respectively. **c** and **d** exhibit typical gapped and nodal-point band structures under CSNES, respectively. In **d**, topological charge is defined on the yellow loop surrounding the nodal point.

classification theory for CSNES. The key step is to identify the classifying space for a CSNES. Our analysis shows that the classifying space is the Stiefel manifold $V_M(\mathbb{C}^N)$, namely the space consisting of all possible sets of M orthonormal vectors in an N -dimensional complex vector space [26, 27]. Here, we assume $N \geq M$ without loss of generality.

As the CSNES can be regarded as a generalization of class AIII in the AZ classes, we further consider space-

time inversion symmetry \mathcal{PT} to extend CSNES [28–36]. We identify totally three symmetry classes with the classifying spaces $V_N(\mathbb{C}^N)$, $V_N(\mathbb{R}^N)$ and $V_N(\mathbb{H}^N)$, resembling Dyson’s threefold way [37]. The topological classifications for both gapped and gapless systems are given by the homotopy groups $\pi_d[V_M(\mathbb{F}^N)]$ with $\mathbb{F} = \mathbb{C}, \mathbb{R}$ and \mathbb{H} . For gapped systems, d is just the spatial dimensionality, while for gapless systems d corresponds to the spatial codimension of the gapless modes [19, 20, 38] (Fig. 1d).

As an important application, the classification theory is applied to clarify the topological invariant of the Po-Zou-Senthil-Vishwanath (PZSV) model, which captures the essential physics of various Morie systems [2, 12]. We further demonstrate our theory by constructing a 3D topological insulator on the Lieb lattice model corresponding to the unit element of $\pi_3[V_1(\mathbb{C}^2)] \cong \mathbb{Z}$, a 1D topological insulator and a 2D topological semimetal on dice lattices corresponding to the nontrivial element of $\pi_1[V_1(\mathbb{R}^2)] \cong \mathbb{Z}_2$.

The general sublattice symmetry Let us start with formulating the sublattice symmetry. On a bipartite lattice, the sublattice symmetry is essentially a \mathbb{Z}_2 gauge transformation:

$$S : |i\rangle \mapsto (-1)^{s(i)} |i\rangle, \quad (1)$$

where $s(i) = 0$ or 1 for i being a A -site or B -site, respectively. Let M and N be the site numbers of A -sites and B -sites in each unit cell. The sublattice symmetry operator S is represented in momentum space as

$$S = \begin{bmatrix} 1_M & \\ & -1_N \end{bmatrix} \quad (2)$$

with 1_n being the $n \times n$ identity matrix.

A real-space Hamiltonian H preserves the sublattice symmetry if it solely consists of hopping terms between the two sublattices, i.e., $H = \sum_{ij} t_{ij} |i\rangle\langle j|$ with $i \in A$ and $j \in B$ for each $t_{ij} |i\rangle\langle j|$. It is clear that the gauge transformation (1) inverses every hopping term $t_{ij} \mapsto -t_{ij}$, and therefore inverses the Hamiltonian H . Accordingly, the momentum-space Hamiltonian $\mathcal{H}(\mathbf{k})$ satisfies $S\mathcal{H}(\mathbf{k})S^\dagger = -\mathcal{H}(\mathbf{k})$, which may be more elegantly expressed as the anti-commutation relation,

$$\{\mathcal{H}(\mathbf{k}), S\} = 0. \quad (3)$$

The anti-commutation relation (3) requires the Hamiltonian be in the anti-diagonal form,

$$\mathcal{H}(\mathbf{k}) = \begin{bmatrix} & \mathcal{Q}(\mathbf{k}) \\ \mathcal{Q}^\dagger(\mathbf{k}) & \end{bmatrix}, \quad (4)$$

where $\mathcal{Q}(\mathbf{k})$ is an $M \times N$ matrix and therefore $\mathcal{Q}^\dagger(\mathbf{k}) := [\mathcal{Q}(\mathbf{k})]^\dagger$ an $N \times M$ matrix.

The spectrum of $\mathcal{H}(\mathbf{k})$ in the anti-diagonal form is determined by the singular values of $\mathcal{Q}(\mathbf{k})$. To see this, we first perform the singular value decomposition

$$\mathcal{Q}(\mathbf{k}) = \mathcal{V}(\mathbf{k})\mathcal{D}(\mathbf{k})\mathcal{U}^\dagger(\mathbf{k}). \quad (5)$$

$(\mathcal{PT})^2$	$V_M(\mathbb{K}^N)$	$N - M$	$d = 1$	$d = 2$	$d = 3$
0	$V_M(\mathbb{C}^N)$	0	\mathbb{Z}	0	\mathbb{Z}
		1	0	0	\mathbb{Z}
1	$V_M(\mathbb{R}^N)$	0	\mathbb{Z}_2	0	\mathbb{Z}
		1	\mathbb{Z}_2	0	\mathbb{Z}
		2	0	$2\mathbb{Z}$	\mathbb{Z}
		3	0	0	\mathbb{Z}_2
-1	$V_M(\mathbb{H}^N)$	0	0	0	\mathbb{Z}

TABLE I. Topological classification table of the Stiefel manifolds. The first column specifies the three cases of \mathcal{PT} symmetry, which determines the classifying space $V_M(\mathbb{K}^N)$. Here, $(\mathcal{PT})^2 = 0$ indicates the absence of \mathcal{PT} symmetry. For each classifying space, $N - M$ is fixed at various values while N and M are presumed to be sufficiently large. The corresponding homotopy groups $\pi_d(V_M(\mathbb{K}^N))$ are presented for $d = 1, 2, 3$. Note that $\pi_d(V_M(\mathbb{K}^N)) = 0$ if $N - M$ is greater than the exhibited range.

Here, \mathcal{V} and \mathcal{U} are square matrices with rank M and N , respectively. \mathcal{D} is an $M \times N$ matrix of the form $\mathcal{D} = [\Lambda, \mathbf{0}]$, where Λ is a diagonal $M \times M$ square matrix and $\mathbf{0}$ the zero $M \times (N - M)$ matrix. The diagonal entries of Λ are just the singular values λ_i of \mathcal{Q} with $\lambda_i \geq 0$. Then, the Hamiltonian $\mathcal{H}(\mathbf{k})$ can be expressed in the decomposition form,

$$\mathcal{H}(\mathbf{k}) = \begin{bmatrix} \mathcal{V} & \\ & \mathcal{U} \end{bmatrix} \begin{bmatrix} & \mathcal{D}(\mathbf{k}) \\ \mathcal{D}^\dagger(\mathbf{k}) & \end{bmatrix} \begin{bmatrix} \mathcal{V}^\dagger & \\ & \mathcal{U}^\dagger \end{bmatrix}. \quad (6)$$

Then, the spectrum of $\mathcal{H}(\mathbf{k})$ can be read off as

$$\lambda_1(\mathbf{k}), -\lambda_1(\mathbf{k}), \dots, \lambda_M(\mathbf{k}), -\lambda_M(\mathbf{k}), 0, \dots, 0, \quad (7)$$

with $N - M$ zeros. Each single value λ_i contributes a pair of eigen energies $\pm\lambda_i$. Thus, we observe a feature of the CSNES, i.e., generically there exist $|N - M|$ flat bands at the zero energy.

The classifying spaces We then proceed to derive the classifying spaces. For the tenfold symmetry classes, this is done by considering a one-point symmetry-preserving Hamiltonian, where an energy gap is assumed at zero energy and eigen energies are flattened to be ± 1 . Here, with the $|N - M|$ zero modes for the one-point Hamiltonian \mathcal{H} with the CSNES, we assume two energy gaps below and above the zero energy and flatten positive and negative eigen energies as ± 1 , respectively.

The assumption of two energy gaps means all singular values of \mathcal{Q} are nonzero, and the flattening of the spectrum of \mathcal{H} is equivalent to the flattening of all singular values of \mathcal{Q} to 1. Let $\tilde{\mathcal{O}}$ denote the flattened version of any operator \mathcal{O} . Then, $\tilde{\Lambda} = 1_M$, and $\tilde{\mathcal{D}} = (1_M, 0_{M \times (N - M)})$. Consequently,

$$\tilde{\mathcal{Q}} = \mathcal{V}[1_M, \mathbf{0}]\mathcal{U}^\dagger = [1_M, \mathbf{0}] \begin{bmatrix} \mathcal{V} & \\ & 1_{N - M} \end{bmatrix} \mathcal{U}^\dagger. \quad (8)$$

Hence, any \mathcal{Q} can be flattened to the form,

$$\tilde{\mathcal{Q}} = [1_M, \mathbf{0}]\mathcal{W}, \quad (9)$$

where \mathcal{W} can be any $N \times N$ unitary matrix, namely $\mathcal{W} \in \text{U}(N)$.

Let us look into the geometric meaning of Eq. (9). The i th row of \mathcal{W} is a vector v_i in the space \mathbb{C}^N , and all the N vectors v_i form an orthonormal basis of \mathbb{C}^N , i.e., $(v_i, v_j) = \delta_{ij}$. The multiplication by $[1_M, \mathbf{0}]$ on the left side of \mathcal{W} just selects the first M rows, namely the first M vectors v_i with $i = 1, 2, \dots, M$. Since \mathcal{W} can exhaust all possible orthonormal bases of \mathbb{C}^N , the space of \mathcal{Q} is just the space of all possible M orthonormal vectors in \mathbb{C}^N , which is just the definition of the Stiefel manifold denoted by $V_M(\mathbb{C}^N)$. Thus, the classifying space of the CSNES is just the complex Stiefel manifold $V_M(\mathbb{C}^N)$.

It is significant to notice that \mathcal{W} is not uniquely determined by $\tilde{\mathcal{Q}}$, because $\tilde{\mathcal{Q}}$ is invariant under the transformation,

$$\mathcal{W} \mapsto \begin{bmatrix} 1_M & \\ & \mathcal{G} \end{bmatrix} \mathcal{W}, \quad (10)$$

for any unitary matrix $\mathcal{G} \in \text{U}(N - M)$. The inverse is also true. If \mathcal{W} and \mathcal{W}' corresponds to the same $\tilde{\mathcal{Q}}$, there exists a unitary matrix $\mathcal{G} \in \text{U}(N - M)$ with $\mathcal{W}' = \text{diag}[1_M, \mathcal{G}]\mathcal{W}$. Thus, we obtain the representation of the complex Stiefel manifold,

$$V_M(\mathbb{C}^N) = \text{U}(N)/\text{U}(N - M). \quad (11)$$

The special case of $V_N(\mathbb{C}^N) = \text{U}(N)$ agrees with the classifying space of class AIII in the tenfold symmetry classes.

The topological classifications are given by the homotopy groups $\pi_d[V_M(\mathbb{C}^N)]$ as aforementioned. For a fixed value of $N - M$ and a given d , $\pi_d[V_M(\mathbb{C}^N)]$ will stabilize to a fixed group if M surpasses a threshold value. This is the so-called the stability of homotopy groups. The stable homotopy groups for physical dimensions are tabulated in Tab. I. See the SM for derivation details [39].

The threefold way of classifying spaces We then include \mathcal{PT} symmetry into consideration to generalize the five chiral AZ classes with ordinary sublattice symmetry. Besides class AIII with only the chiral symmetry, the other four are specified by $(\mathcal{PT})^2 = \pm 1$ and $\mathcal{PTS} = \pm \mathcal{SPT}$. For the later, which commutation relation is satisfied is determined by whether inversion exchanges the two sublattices. But, for CSNES, the two sublattices cannot be exchanged, since they have different site numbers in each unit cell. Then, only the commutation relation $\mathcal{PTS} = \mathcal{SPT}$ is allowed. Then, there exist only two possibilities, namely $(\mathcal{PT})^2 = \pm 1$.

For $(\mathcal{PT})^2 = 1$, the operator can always be represented as $\mathcal{PT} = \mathcal{K}$ with \mathcal{K} the complex conjugation. With $\mathcal{PT} = \mathcal{K}$, \mathcal{H} becomes a real symmetric matrix, and the Hilbert space is essentially a real space \mathbb{R}^N . Accordingly, the classifying space is the real Stiefel manifold,

$$V_M(\mathbb{R}^N) = \text{O}(N)/\text{O}(N - M). \quad (12)$$

For $(\mathcal{PT})^2 = -1$, each energy band bears the Kramers degeneracy, and the \mathcal{PT} operator can be represented as $\mathcal{PT} = -i\sigma_2\mathcal{K}$ with the Pauli matrix σ_2 acting in the twofold degenerate space. $\mathcal{PT} = -i\sigma_2\mathcal{K}$ together with the imaginary unit i form generators of the quaternionic field \mathbb{H} . Hence, the classifying space is the quaternionic Stiefel manifold,

$$V_M(\mathbb{H}^N) = \text{Sp}(N)/\text{Sp}(N - M). \quad (13)$$

The stable homotopy groups of real and quaternionic Stiefel manifolds are tabulated in Tab. I, and the derivation details are provided in the SM [39]. The three classifying spaces resemble Dyson's threefold way for symmetry classes [37].

Application and demonstration The PZSV model for various Morie systems features CSNES that leads to the zero-energy flat bands and \mathcal{PT} symmetry for the real band structure. Therefore, the model well fits into our framework. The classifying space is $V_M(\mathbb{R}^N)$, and the corresponding homotopy group is $\pi_2(V_M[\mathbb{R}^N]) \cong 2\mathbb{Z}$ with $N - M = 2$. The detailed analysis of the model is quite technical and can be found in the SM [39]. The result is that the model does represent nontrivial topology of the classification.

We now present models for simple and clear demonstration of the topological classifications in Tab. I.

3D topological insulator According to Tab. I, the homotopy group $\pi_3[V_{N-1}(\mathbb{C}^N)] \cong \mathbb{Z}$ means there exist 3D chiral symmetric topological insulators with A -sites one more than B -sites in each unit cell.

Such a model is constructed on the 3D lattice as a stack of layers of Lieb lattices, where each unit cell contains one A -site and two B -sites as illustrated in Fig. 2a. The Hamiltonian is given by

$$\mathcal{H}_{3D}(\mathbf{k}) = \begin{bmatrix} 0 & w_1(\mathbf{k}) & w_2(\mathbf{k}) \\ w_1^*(\mathbf{k}) & 0 & 0 \\ w_2^*(\mathbf{k}) & 0 & 0 \end{bmatrix}, \quad (14)$$

where $w_1(\mathbf{k}) = t + t'e^{ik_x} + J_1e^{-ik_y} + J_2e^{-ik_z}$ and $w_2(\mathbf{k}) = t + t'e^{ik_y} + 2J_1 \cos k_z$.

Since hopping occurs only between different sublattices, the CSNES, represented by $\mathcal{S} = \text{diag}[1, -1_2]$, is preserved. The energy spectrum of $\mathcal{H}_{3D}(\mathbf{k})$ can be derived as $\{0, \lambda(\mathbf{k}), -\lambda(\mathbf{k})\}$ with $\lambda(\mathbf{k}) = (|w_1|^2 + |w_2|^2)^{1/2}$. We observe that the band structure features two gaps separated by a flat band at the zero energy for the parameters given in the caption of Fig. 2c.

From the derivation of the topological classification in the SM [39], we learn that the topological invariant \mathcal{N} is just the winding number of $\mathcal{W}(\mathbf{k})$ defined in Eq. (9), i.e.,

$$\mathcal{N} = \frac{1}{24\pi^2} \int_{\text{BZ}} d^3k \epsilon^{ijk} \text{tr} \mathcal{W} \partial_i \mathcal{W}^\dagger \mathcal{W} \partial_j \mathcal{W}^\dagger \mathcal{W} \partial_k \mathcal{W}^\dagger, \quad (15)$$

where ϵ^{ijk} is the completely antisymmetric tensor.

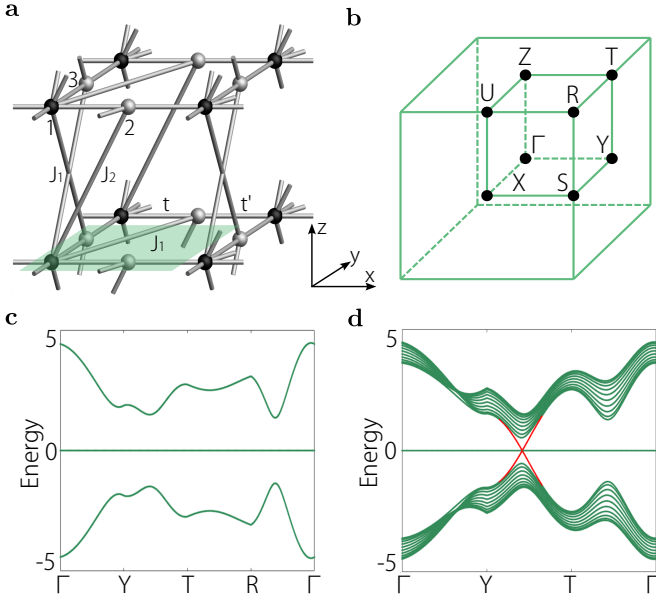


FIG. 2. **a** The 3D lattice model as a stack of layers of Lieb lattices. Each unit cell contains one A -site and two B -sites marked in black and grey, respectively. **b** The Brillouin zone (BZ) with high-symmetry points marked. **c** The bulk band structure along the path specified by the high symmetry points. **d** The band structure with a boundary opened normal to the x direction. It is plotted along the path specified by the high symmetry points in the boundary BZ. The boundary states are marked in red. We set $t = 0.5$, $t' = 1$, $J_1 = 1$ and $J_2 = i$.

Particularly, for our model (14), $\mathcal{W}(\mathbf{k}) = d_0\sigma_0 - i\sum_{i=1}^3 d_i\sigma_i$, where $d_0 = \text{Re}(w_1/\lambda)$, $d_1 = \text{Im}(w_2/\lambda)$, $d_2 = \text{Re}(w_2/\lambda)$, $d_3 = \text{Im}(w_1/\lambda)$, $\sigma_0 = 1_2$ and σ_i are the Pauli matrices. Then, d_μ is just a vector on the unit sphere S^3 , and \mathcal{N} is just the winding number of the unit vector d_μ wrapping over the Brillouin zone, i.e., $\mathcal{N} = \frac{1}{2\pi^2} \int_{T^3} d^3k \epsilon^{\mu\nu\rho\lambda} d_\mu \partial_{k_1} d_\nu \partial_{k_2} d_\rho \partial_{k_3} d_\lambda$. For the parameter values in Fig. 2c, we obtain $\mathcal{N} = -1$.

The nontrivial topological invariant leads to boundary bands across the two energy gaps, which connect the states in the 3D bulk bands. This is shown in Fig. 2d, where the boundary is opened perpendicular to the x direction.

2D topological semimetal with PT symmetry The homotopy group $\pi_1[V_{N-1}(\mathbb{R}^N)] \cong \mathbb{Z}_2$ in Tab. I indicates that there exist 1D topological insulator, 2D topological nodal point and 3D topological nodal line, protected by CSNES and \mathcal{PT} symmetry without spin-orbit coupling. A model for the 1D topological insulator can be found in the SM [39], and we present a 2D topological semimetal on the dice lattice here.

As illustrated in Fig. 3a, each unit cell contains one A -site and two B -sites, and symmetry operators are represented as $\mathcal{S} = \text{diag}[1, -1_2]$ and $\mathcal{PT} = \text{diag}[1, \sigma_1]\mathcal{K}$. The \mathcal{PT} symmetry is in the form because the inversion symmetry is centered at the A -site and exchanges two

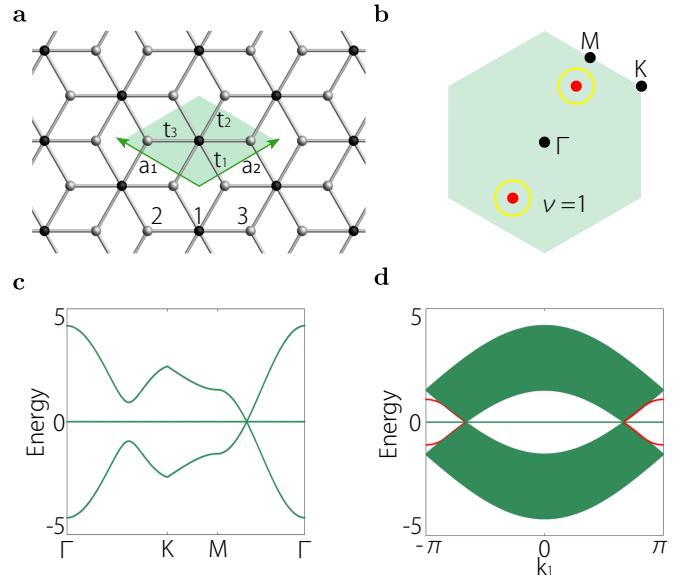


FIG. 3. **a** The dice lattice structure. A -sites and B -sites are marked in black and grey, respectively, and the unit cell is indicated by the shadowed parallelogram. \mathbf{a}_1 and \mathbf{a}_2 denote the two unit lattice vectors. **b** The Brillouin zone. The two nodal points are highlighted as two red dots, and high symmetry points are marked as black dots. **c** The bulk band structure along the $\Gamma - K - M - \Gamma$ line in **b**. **d** The band structure along a boundary opened parallel to \mathbf{a}_1 direction. The edge Fermi arcs are marked in red. We set $t_1 = t_2 = t_3 = 1$.

B -sites. The Hamiltonian is given by

$$\mathcal{H}_{2D}(\mathbf{k}) = w(\mathbf{k})S_+ + w^*(\mathbf{k})S_-, \quad (16)$$

where $w(\mathbf{k}) = t_3 + t_1 e^{-i\mathbf{k}\cdot\mathbf{a}_1} + t_2 e^{i\mathbf{k}\cdot\mathbf{a}_2}$. Here, $S_\pm = (S_x \pm iS_y)/\sqrt{2}$, where S_i are the spin-1 operators with the explicit matrix representation given in the SM [39]. Hamiltonians in this form are called Maxwell Hamiltonians [40–42]. Notably, the Hamiltonian resembles that of graphene with σ_\pm replaced by S_\pm .

The energy spectrum is derived as $0, \pm\sqrt{2}|w(\mathbf{k})|$, resembling that of graphene with an additional flat band at zero energy. Hence, it generically corresponds to a semimetal with two nodal points at $\pm\mathbf{K}$ [see Fig. 3b], each now featuring threefold degeneracy. The $\mathbf{k} \cdot \mathbf{p}$ model at \mathbf{K} is given by

$$h(\mathbf{q}) = vq_+ S_+ + vq_- S_- \quad (17)$$

with $q_\pm = (v_x q_x \pm i v_y q_y)/v$. Here, $\mathbf{q} = \mathbf{k} - \mathbf{K}$. The parameters v_x and v_y are determined by t_i , and $v = (v_x^2 + v_y^2)^{1/2}$. The $\mathbf{k} \cdot \mathbf{p}$ model at $-\mathbf{K}$ is related to $h(\mathbf{q})$ by time-reversal symmetry.

To formulate the topological charge, we first perform a unitary transformation $U = \text{diag}[1, e^{-i\pi/4}, e^{i\pi\sigma_1/4}]$ with $U\mathcal{PT}U^\dagger = \mathcal{K}$. Then, we obtain the real Hamiltonian $\mathcal{H}_{2D}^R(\mathbf{k}) = U\mathcal{H}_{2D}(\mathbf{k})U^\dagger = \sqrt{2}w_+(\mathbf{k})S_+ + \sqrt{2}w_-(\mathbf{k})S_-$ with $w_\pm = (\text{Re}w \pm \text{Im}w)/\sqrt{2}$. The topological charge of

each nodal point is formulated on a circle S^1 enclosing \mathbf{K} [see Fig. 3b]. Since $\mathcal{H}_{2D}^{\mathbb{R}}(\phi)$ with $\phi \in S^1$ is gapped, we can derive $\mathcal{W}(\phi) \in O(2)$ defined in Eq. (9) from $\mathcal{H}_{2D}^{\mathbb{R}}(\phi)$. The topological charge is just the winding number of \mathcal{W} as a map from S^1 to $O(2)$, i.e.,

$$\nu = \frac{1}{4\pi} \int_{S^1} d\phi \operatorname{tr} J \mathcal{W} \partial_{\phi} \mathcal{W}^T \pmod{2} \quad (18)$$

with the $SO(2)$ generator $J = i\sigma_2$. Particularly, for our model $\mathcal{W}(\phi) = [w_+(\phi)\sigma_1 + w_-(\phi)\sigma_3]/|w(\phi)|$ leads to the nontrivial topological charge $\nu = 1$.

Summary In summary, we have established the theoretical foundation to study topological structures protected by CSNES. As bipartite lattices with CSNES widely exist, our work can be broadly applied to reveal novel topologies in crystalline systems with CSNES. Particularly, our theory has been applied to clarify the topological invariant of the PZSV model with both CSNES and PT symmetry. Models constructed here can be readily realized by various artificial crystals [14, 43–52], and can pave the way for the further experimental investigation of novel topologies with CSNES.

* yuxinphy@hku.hk

- [1] N. Regnault, Y. Xu, M.-R. Li, D.-S. Ma, M. Jovanovic, A. Yazdani, S. S. Parkin, C. Felser, L. M. Schoop, N. P. Ong, *et al.*, *Nature* **603**, 824 (2022).
- [2] D. Călugăru, A. Chew, L. Elcoro, Y. Xu, N. Regnault, Z.-D. Song, and B. A. Bernevig, *Nature Physics* **18**, 185 (2022).
- [3] S. Taie, T. Ichinose, H. Ozawa, and Y. Takahashi, *Nature Communications* **11**, 257 (2020).
- [4] M. R. Slot, T. S. Gardenier, P. H. Jacobse, G. C. Van Miert, S. N. Kempkes, S. J. Zevenhuizen, C. M. Smith, D. Vanmaekelbergh, and I. Swart, *Nature physics* **13**, 672 (2017).
- [5] R. A. Vicencio, C. Cantillano, L. Morales-Inostroza, B. Real, C. Mejía-Cortés, S. Weimann, A. Szameit, and M. I. Molina, *Phys. Rev. Lett.* **114**, 245503 (2015).
- [6] S. Mukherjee, A. Spracklen, D. Choudhury, N. Goldman, P. Öhberg, E. Andersson, and R. R. Thomson, *Phys. Rev. Lett.* **114**, 245504 (2015).
- [7] S. Xia, A. Ramachandran, S. Xia, D. Li, X. Liu, L. Tang, Y. Hu, D. Song, J. Xu, D. Leykam, S. Flach, and Z. Chen, *Phys. Rev. Lett.* **121**, 263902 (2018).
- [8] A. Julku, S. Peotta, T. I. Vanhala, D.-H. Kim, and P. Törmä, *Phys. Rev. Lett.* **117**, 045303 (2016).
- [9] T. Andrijauskas, E. Anisimovas, M. Račiūnas, A. Mekys, V. Kudriašov, I. B. Spielman, and G. Juzeliūnas, *Phys. Rev. A* **92**, 033617 (2015).
- [10] N. Mohanta, R. Soni, S. Okamoto, and E. Dagotto, *Communications Physics* **6**, 240 (2023).
- [11] F. Wang and Y. Ran, *Phys. Rev. B* **84**, 241103 (2011).
- [12] H. C. Po, L. Zou, T. Senthil, and A. Vishwanath, *Phys. Rev. B* **99**, 195455 (2019).
- [13] A. Graf and F. Piéchon, *Phys. Rev. B* **108**, 115105 (2023).
- [14] Q. Mo, R. Zheng, C. Lu, X. Huang, Z. Liu, and S. Zhang, arXiv preprint arXiv:2405.07569 (2024).
- [15] A. P. Schnyder, S. Ryu, A. Furusaki, and A. W. W. Ludwig, *Phys. Rev. B* **78**, 195125 (2008).
- [16] M. F. Atiyah, *The Quarterly Journal of Mathematics* **17**, 367 (1966).
- [17] A. Kitaev, *AIP Conference Proceedings* **1134**, 22 (2010).
- [18] A. Altland and M. R. Zirnbauer, *Phys. Rev. B* **55**, 1142 (1997).
- [19] Y. X. Zhao and Z. D. Wang, *Phys. Rev. Lett.* **110**, 240404 (2013).
- [20] G. E. Volovik, *Universe in a helium droplet* (Oxford University Press, Oxford UK, 2003).
- [21] X.-L. Qi and S.-C. Zhang, *Rev. Mod. Phys.* **83**, 1057 (2011).
- [22] S.-Q. Shen, *Topological Insulators: Dirac Equation in Condensed Matters* (Springer, 2012) pp. 15–17.
- [23] M. Z. Hasan and C. L. Kane, *Rev. Mod. Phys.* **82**, 3045 (2010).
- [24] C.-K. Chiu, J. C. Y. Teo, A. P. Schnyder, and S. Ryu, *Rev. Mod. Phys.* **88**, 035005 (2016).
- [25] J. C. Y. Teo and C. L. Kane, *Phys. Rev. B* **82**, 115120 (2010).
- [26] J. IM, *The Topology of Stiefel Manifolds* (Cambridge University Press, 1977).
- [27] See the wikipedia item: https://en.wikipedia.org/wiki/Stiefel_manifold.
- [28] K. Wang, J.-X. Dai, L. B. Shao, S. A. Yang, and Y. X. Zhao, *Phys. Rev. Lett.* **125**, 126403 (2020).
- [29] Y. X. Zhao, A. P. Schnyder, and Z. D. Wang, *Phys. Rev. Lett.* **116**, 156402 (2016).
- [30] Y. X. Zhao and Y. Lu, *Phys. Rev. Lett.* **118**, 056401 (2017).
- [31] J. Ahn, D. Kim, Y. Kim, and B.-J. Yang, *Phys. Rev. Lett.* **121**, 106403 (2018).
- [32] J. Ahn, S. Park, and B.-J. Yang, *Phys. Rev. X* **9**, 021013 (2019).
- [33] T. Bzdusek and M. Sigrist, *Phys. Rev. B* **96**, 155105 (2017).
- [34] H. Xue, Z. Chen, Z. Cheng, J. Dai, Y. Long, Y. Zhao, and B. Zhang, *Nature Communications* **14** (2023).
- [35] J.-X. Dai, K. Wang, S. A. Yang, and Y. X. Zhao, *Phys. Rev. B* **104**, 165142 (2021).
- [36] X.-L. Sheng, C. Chen, H. Liu, Z. Chen, Z.-M. Yu, Y. X. Zhao, and S. A. Yang, *Phys. Rev. Lett.* **123**, 256402 (2019).
- [37] F. J. Dyson, *Journal of Mathematical Physics* **3**, 1199 (1962).
- [38] The codimension is defined as the dimensionality of the sphere S^d enclosing the gapless modes from their transverse dimensions in momentum space.
- [39] See the Supplemental Material for topological classifications, topological invariants, matrix representation of spin-1 operators, a 1D insulator model with CSNES and \mathcal{PT} symmetry, and ten-band PZSV lattice model with CSNES and \mathcal{PT} symmetry.
- [40] Y.-Q. Zhu, D.-W. Zhang, H. Yan, D.-Y. Xing, and S.-L. Zhu, *Phys. Rev. A* **96**, 033634 (2017).
- [41] X. Tan, D.-W. Zhang, Q. Liu, G. Xue, H.-F. Yu, Y.-Q. Zhu, H. Yan, S.-L. Zhu, and Y. Yu, *Phys. Rev. Lett.* **120**, 130503 (2018).
- [42] M. Stone, *International Journal of Modern Physics B* **30**, 1550249 (2016).
- [43] D.-W. Zhang, Y.-Q. Zhu, Y. X. Zhao, H. Yan, and S.-L.

- Zhu, *Advances in Physics* **67**, 253 (2018).
- [44] R. Yu, Y. X. Zhao, and A. P. Schnyder, *National Science Review* (2020), nwa065.
- [45] T. Ozawa, H. M. Price, A. Amo, N. Goldman, M. Hafezi, L. Lu, M. C. Rechtsman, D. Schuster, J. Simon, O. Zeitlinger, and I. Carusotto, *Rev. Mod. Phys.* **91**, 015006 (2019).
- [46] C. W. Peterson, W. A. Benalcazar, T. L. Hughes, and G. Bahl, *Nature* **555**, 346 (2018).
- [47] M. Serra-Garcia, V. Peri, R. Süsstrunk, O. R. Bilal, T. Larsen, L. G. Villanueva, and S. D. Huber, *Nature* **555**, 342 (2018).
- [48] G. G. Liu, Z. Gao, Q. Wang, X. Xi, Y. H. Hu, M. Wang, C. Liu, X. Lin, L. Deng, S. A. Yang, P. Zhou, Y. Yang, Y. Chong, and B. Zhang, *Nature* **609**, 925 (2022).
- [49] Z. Yang, F. Gao, X. Shi, X. Lin, Z. Gao, Y. Chong, and B. Zhang, *Phys. Rev. Lett.* **114**, 114301 (2015).
- [50] H. Xue, Y. Yang, and B. Zhang, *Nature Reviews Materials* **7**, 974 (2022).
- [51] L. Lu, J. D. Joannopoulos, and M. Soljačić, *Nature photonics* **8**, 821 (2014).
- [52] S. D. Huber, *Nature Physics* **12**, 621 (2016).

The Supplemental Materials for “Topological classification of chiral symmetry with non-equal sublattices”

J. X. Dai^{1,2} and Y. X. Zhao^{1,2,*}

¹*Department of Physics and HKU-UCAS Joint Institute for Theoretical and Computational Physics at Hong Kong, The University of Hong Kong, Pokfulam Road, Hong Kong, China*

²*HK Institute of Quantum Science & Technology, The University of Hong Kong, Pokfulam Road, Hong Kong, China*

I. Topological classifications

a. The classifying space: Stiefel manifolds

In our manuscript, we discuss bipartite systems that maintain chiral symmetry across non-equal sublattices, referred to as chiral symmetry with non-equal sublattices (CSNES). The CSNE operator can be represented by

$$\mathcal{S} = \begin{bmatrix} 1_M & 0 \\ 0 & -1_N \end{bmatrix}. \quad (\text{S1})$$

Here, we assume $M < N$ without loss of generality for subsequent discussions. The Hamiltonian $\mathcal{H}(\mathbf{k})$ and the operator \mathcal{S} satisfy an anti-commutation relation, which restricts $\mathcal{H}(\mathbf{k})$ to an anti-diagonal form

$$\mathcal{H}(\mathbf{k}) = \begin{bmatrix} & \mathcal{Q}(\mathbf{k}) \\ \mathcal{Q}^\dagger(\mathbf{k}) & \end{bmatrix}. \quad (\text{S2})$$

In this equation, $\mathcal{Q}(\mathbf{k})$ is an $M \times N$ matrix and $\mathcal{Q}^\dagger(\mathbf{k})$ is its conjugate transpose, an $N \times M$ matrix.

The matrix $\mathcal{Q}(\mathbf{k})$ can be factorized via its singular value decomposition (SVD) as:

$$\mathcal{Q}(\mathbf{k}) = \mathcal{V}(\mathbf{k})\mathcal{D}(\mathbf{k})\mathcal{U}^\dagger(\mathbf{k}). \quad (\text{S3})$$

Here, \mathcal{V} and \mathcal{U} are unitary matrices of rank M and N , respectively. The matrix \mathcal{D} is of size $M \times N$ and structured as $\mathcal{D} = [\Lambda, \mathbf{0}]$, where Λ is a diagonal $M \times M$ matrix and $\mathbf{0}$ is a zero $M \times (N - M)$ matrix. The diagonal entries of Λ are the singular values λ_i of \mathcal{Q} , where $\lambda_i \geq 0$. Utilizing the SVD, the Hamiltonian $\mathcal{H}(\mathbf{k})$ can be expressed in decomposed form,

$$\mathcal{H}(\mathbf{k}) = \begin{bmatrix} \mathcal{V}(\mathbf{k}) & \\ & \mathcal{U}(\mathbf{k}) \end{bmatrix} \begin{bmatrix} \mathcal{D}^\dagger(\mathbf{k}) & \\ & \mathcal{D}(\mathbf{k}) \end{bmatrix} \begin{bmatrix} \mathcal{V}^\dagger(\mathbf{k}) & \\ & \mathcal{U}^\dagger(\mathbf{k}) \end{bmatrix}. \quad (\text{S4})$$

This decomposition implies that each singular value λ_i contributes a pair of eigenvalues $\pm\lambda_i$ to $\mathcal{H}(\mathbf{k})$.

To analyze the topological properties of $\mathcal{H}(\mathbf{k})$, we transform it into its flattened version $\tilde{\mathcal{H}}(\mathbf{k})$ by continuously deforming the eigenvalues $\lambda_i(\mathbf{k})$ to 1. In this flattened representation, the eigenvalues of $\mathcal{H}(\mathbf{k})$ are confined to 0 and ± 1 . We denote the flattened version of any operator \mathcal{O} as $\tilde{\mathcal{O}}$. Specially, for $\mathcal{H}(\mathbf{k})$, we have $\tilde{\Lambda} = 1_M$ and $\tilde{\mathcal{D}} = (1_M, 0_{M \times (N-M)})$. Consequently, we can express $\tilde{\mathcal{Q}}$ as:

$$\tilde{\mathcal{Q}} = [1_M, \mathbf{0}] \begin{bmatrix} \mathcal{V} & \\ & 1_{N-M} \end{bmatrix} \mathcal{U}^\dagger. \quad (\text{S5})$$

Therefore, any \mathcal{Q} can be represented in its flattened form:

$$\tilde{\mathcal{Q}} = [1_M, \mathbf{0}]\mathcal{W}, \quad (\text{S6})$$

*yuxinphy@hku.hk

$(\mathcal{PT})^2$	$V_M(\mathbb{K}^N)$	$N - M$	$d = 1$	$d = 2$	$d = 3$
0	$V_M(\mathbb{C}^N)$	0	\mathbb{Z}	0	\mathbb{Z}
		1	0	0	\mathbb{Z}
1	$V_M(\mathbb{R}^N)$	0	\mathbb{Z}_2	0	\mathbb{Z}
		1	\mathbb{Z}_2	0	\mathbb{Z}
		2	0	$2\mathbb{Z}$	\mathbb{Z}
		3	0	0	\mathbb{Z}_2
-1	$V_M(\mathbb{H}^N)$	0	0	0	\mathbb{Z}

TABLE I: Topological classification table of the Stiefel manifolds. The first column specifies the three cases of \mathcal{PT} symmetry, which determines the classifying space $V_M[\mathbb{K}^N]$. Here, $(\mathcal{PT})^2 = 0$ indicates the absence of \mathcal{PT} symmetry. For each classifying space, $N - M$ is fixed at various values while N and M are presumed to be sufficiently large. The corresponding homotopy groups $\pi_d(V_M(\mathbb{K}^N))$ are presented for $d = 1, 2, 3$. Note that $\pi_d[V_M(\mathbb{K}^N)] = 0$ if $N - M$ is greater than the exhibited range.

where \mathcal{W} can be any $N \times N$ unitary matrix, i.e., $\mathcal{W} \in \text{U}(N)$. It is crucial to recognize that \mathcal{W} is not uniquely determined by $\tilde{\mathcal{Q}}$, as $\tilde{\mathcal{Q}}$ is invariant under the transformation

$$\mathcal{W} \mapsto \begin{bmatrix} 1_M & \\ & \mathcal{G} \end{bmatrix} \mathcal{W}, \quad (\text{S7})$$

where \mathcal{G} is any unitary matrix with rank $N - M$, i.e., $\mathcal{G} \in \text{U}(N - M)$. The inverse is also true. If \mathcal{W} and \mathcal{W}' correspond to the same $\tilde{\mathcal{Q}}$, there exists a unitary matrix $\mathcal{G} \in \text{U}(N - M)$ with $\mathcal{W}' = \text{diag}[1_M, \mathcal{G}]\mathcal{W}$. Thus, we obtain the representation of the complex Stiefel manifold

$$V_M(\mathbb{C}^N) = \text{U}(N)/\text{U}(N - M). \quad (\text{S8})$$

If the spacetime inversion symmetry \mathcal{PT} with $(\mathcal{PT})^2 = 1$ [$(\mathcal{PT})^2 = -1$] is added on the bipartite system, \mathcal{W} in Eq. (S6) and \mathcal{G} in Eq. (S7) would be real orthogonal (symplectic) matrices. And the classifying space would become the real (quaternionic) Stiefel manifold $V_M(\mathbb{R}^N)$ [$V_M(\mathbb{H}^N)$], with

$$V_M(\mathbb{R}^N) = \text{O}(N)/\text{O}(N - M), \quad V_M(\mathbb{H}^N) = \text{Sp}(N)/\text{Sp}(N - M). \quad (\text{S9})$$

The topological classifications of the Stiefel manifolds can be calculated as their homotopy groups. In the following, we would show the calculation details of the homotopy groups of the Stiefel manifolds.

b. Homotopy groups of Stiefel manifolds

It is observed that all Stiefel manifolds take the form of a quotient space X/A . To ascertain the homotopy groups of X/A , we employ the long exact sequence arising from the short exact sequence of the form

$$0 \rightarrow A \rightarrow X \rightarrow X/A \rightarrow 0. \quad (\text{S10})$$

This sequence induces a long exact sequence for homotopy groups:

$$\cdots \rightarrow \pi_n(A) \rightarrow \pi_n(X) \rightarrow \pi_n(X/A) \rightarrow \pi_{n-1}(A) \rightarrow \pi_{n-1}(X) \rightarrow \pi_{n-1}(X/A) \rightarrow \cdots. \quad (\text{S11})$$

Utilizing the sequence (S11), we deduce the topological classifications of the Stiefel manifolds, as illustrated in Table. I. Next, we shall present the calculation details for the homotopy groups of the complex, real, and quaternionic Stiefel manifolds, which are essential for the topological classification.

1. Complex Stiefel manifolds

As shown in Table I, we establish that $\pi_1[V_M(\mathbb{C}^N)] = 0$, $\pi_2[V_M(\mathbb{C}^N)] = 0$, $\pi_3[V_M(\mathbb{C}^N)] = 0$ with $M \leq N - 2$, and $\pi_3[V_{N-1}(\mathbb{C}^N)] \cong \mathbb{Z}$. Now, let us provide the derivation details for these consequences.

- For $\pi_1[V_M(\mathbb{C}^N)]$, the exact sequence is structured as follows:

$$\cdots \rightarrow \pi_1[\mathbb{U}(N-M)] \xrightarrow{i_1} \pi_1[\mathbb{U}(N)] \xrightarrow{i_2} \pi_1[V_M(\mathbb{C}^N)] \xrightarrow{i_3} \pi_0[\mathbb{U}(N-M)] \rightarrow \cdots \quad (\text{S12})$$

Using the fact that the image of i_j equals the kernel of i_{j+1} for exact sequences, we can conclude that

$$\ker(i_3) = \text{im}(i_2) \cong \mathbb{Z}/\ker(i_2) = \mathbb{Z}/\text{im}(i_1) = 0, \quad \text{im}(i_3) = 0. \quad (\text{S13})$$

Here, we utilize the fact that i_1 is an isomorphism from \mathbb{Z} to \mathbb{Z} , which implies $\mathbb{Z}/\text{im}(i_1) = 0$. Equations (S12) and (S13) indicate that i_3 is an isomorphism from $\pi_1[V_M(\mathbb{C}^N)]$ to the trivial group 0. Therefore, we obtain that

$$\pi_1[V_M(\mathbb{C}^N)] = 0. \quad (\text{S14})$$

- For $\pi_2[V_M(\mathbb{C}^N)]$, the exact sequence is structured as follows:

$$\cdots \rightarrow \pi_2[\mathbb{U}(N-M)] \xrightarrow{i_1} \pi_2[\mathbb{U}(N)] \xrightarrow{i_2} \pi_2[V_M(\mathbb{C}^N)] \xrightarrow{i_3} \pi_1[\mathbb{U}(N-M)] \xrightarrow{i_4} \pi_1[\mathbb{U}(N)] \rightarrow \cdots \quad (\text{S15})$$

In this condition, we know that

$$\ker(i_3) = \text{im}(i_2) = 0, \quad \text{im}(i_3) = \ker(i_4) = 0. \quad (\text{S16})$$

Here, we utilize the fact that i_4 is an isomorphism from \mathbb{Z} to \mathbb{Z} , which indicates that $\ker(i_4) = 0$. Then, we obtain that

$$\pi_2[V_M(\mathbb{C}^N)] = 0. \quad (\text{S17})$$

- For $\pi_3[V_M(\mathbb{C}^N)]$ with $M \leq N - 2$, the exact sequence is structured as follows:

$$\cdots \rightarrow \pi_3[\mathbb{U}(N-M)] \xrightarrow{i_1} \pi_3[\mathbb{U}(N)] \xrightarrow{i_2} \pi_3[V_M(\mathbb{C}^N)] \xrightarrow{i_3} \pi_2[\mathbb{U}(N-M)] \rightarrow \cdots \quad (\text{S18})$$

In this condition, we know that

$$\ker(i_3) = \text{im}(i_2) \cong \mathbb{Z}/\ker(i_2) = \mathbb{Z}/\text{im}(i_1) = 0, \quad \text{im}(i_3) = 0. \quad (\text{S19})$$

Here, we utilize the fact that i_1 is an isomorphism from \mathbb{Z} to \mathbb{Z} , which implies $\mathbb{Z}/\text{im}(i_1) = 0$. Then, we obtain that

$$\pi_3[V_M(\mathbb{C}^N)] = 0 \text{ with } M \leq N - 2. \quad (\text{S20})$$

- For $\pi_3[V_{N-1}(\mathbb{C}^N)]$, the exact sequence is structured as follows:

$$\cdots \rightarrow \pi_3[\mathbb{U}(1)] \xrightarrow{i_1} \pi_3[\mathbb{U}(N)] \xrightarrow{i_2} \pi_3[V_{N-1}(\mathbb{C}^N)] \xrightarrow{i_3} \pi_2[\mathbb{U}(1)] \rightarrow \cdots \quad (\text{S21})$$

In this condition, we know that

$$\ker(i_3) = \text{im}(i_2) \cong \mathbb{Z}/\ker(i_2) = \mathbb{Z}/\text{im}(i_1) \cong \mathbb{Z}, \quad \text{im}(i_3) = 0. \quad (\text{S22})$$

Since $\pi_3[V_{N-1}(\mathbb{C}^N)]/\ker(i_3) \cong \text{im}(i_3)$, we obtain that

$$\pi_3[V_{N-1}(\mathbb{C}^N)] \cong \mathbb{Z}. \quad (\text{S23})$$

2. Real Stiefel manifolds

As shown in Table I, we have $\pi_1[V_{N-1}(\mathbb{R}^N)] \cong \mathbb{Z}_2$, $\pi_1[V_M(\mathbb{R}^N)] = 0$ with $M \leq N - 2$, $\pi_2[V_{N-1}(\mathbb{R}^N)] = 0$, $\pi_2[V_{N-2}(\mathbb{R}^N)] \cong 2\mathbb{Z}$, $\pi_2[V_M(\mathbb{R}^N)] = 0$ with $M \leq N - 3$, $\pi_3[V_M(\mathbb{R}^N)] \cong \mathbb{Z}$ with $M \geq N - 2$, $\pi_3[V_{N-3}(\mathbb{R}^N)] \cong \mathbb{Z}_2$, and $\pi_3[V_M(\mathbb{R}^N)] = 0$ with $M \leq N - 4$. Now, let us provide the derivation details for these results.

- For $\pi_1[V_{N-1}(\mathbb{R}^N)]$, the exact sequence can be represented as follows:

$$\cdots \rightarrow \pi_1[\mathcal{O}(1)] \xrightarrow{i_1} \pi_1[\mathcal{O}(N)] \xrightarrow{i_2} \pi_1[V_{N-1}(\mathbb{R}^N)] \xrightarrow{i_3} \pi_0[\mathcal{O}(1)] \xrightarrow{i_4} \pi_0[\mathcal{O}(N)] \rightarrow \cdots . \quad (\text{S24})$$

From this sequence, we can deduce the following relationships:

$$\ker(i_3) = \text{im}(i_2) \cong \mathbb{Z}_2/\ker(i_2) = \mathbb{Z}_2/\text{im}(i_1) \cong \mathbb{Z}_2, \quad \text{im}(i_3) = \ker(i_4) = 0. \quad (\text{S25})$$

We utilize the fact that i_4 is an isomorphism from \mathbb{Z}_2 to \mathbb{Z}_2 , which implies $\ker(i_4) = 0$. Since $\pi_1[V_{N-1}(\mathbb{R}^N)]/\ker(i_3) \cong \text{im}(i_3)$, we can conclude that:

$$\pi_1[V_{N-1}(\mathbb{R}^N)] \cong \mathbb{Z}_2. \quad (\text{S26})$$

- For $\pi_1[V_M(\mathbb{R}^N)]$ with $M \leq N - 2$, the exact sequence can be represented as follows:

$$\cdots \rightarrow \pi_1[\mathcal{O}(N - M)] \xrightarrow{i_1} \pi_1[\mathcal{O}(N)] \xrightarrow{i_2} \pi_1[V_{N-1}(\mathbb{R}^N)] \xrightarrow{i_3} \pi_0[\mathcal{O}(N - M)] \xrightarrow{i_4} \pi_0[\mathcal{O}(N)] \rightarrow \cdots . \quad (\text{S27})$$

From this sequence, we can deduce the following relationships:

$$\ker(i_3) = \text{im}(i_2) \cong \mathbb{Z}_2/\ker(i_2) = \mathbb{Z}_2/\text{im}(i_1) = 0, \quad \text{im}(i_3) = \ker(i_4) = 0. \quad (\text{S28})$$

We utilize the fact that i_1 is an isomorphism from \mathbb{Z}_2 to \mathbb{Z}_2 , which implies $\mathbb{Z}_2/\text{im}(i_1) = 0$. Equation (S28) indicates that:

$$\pi_1[V_M(\mathbb{R}^N)] = 0 \text{ for } M \leq N - 2. \quad (\text{S29})$$

- For $\pi_2[V_{N-1}(\mathbb{R}^N)]$, the exact sequence can be represented as follows:

$$\cdots \rightarrow \pi_2[\mathcal{O}(N)] \xrightarrow{i_1} \pi_2[V_{N-1}(\mathbb{R}^N)] \xrightarrow{i_2} \pi_1[\mathcal{O}(1)] \rightarrow \cdots . \quad (\text{S30})$$

From this sequence, we can deduce the following relationships:

$$\ker(i_2) = \text{im}(i_1) = 0, \quad \text{im}(i_2) = 0. \quad (\text{S31})$$

Equation (S31) indicates that:

$$\pi_2[V_{N-1}(\mathbb{R}^N)] = 0. \quad (\text{S32})$$

- For $\pi_2[V_{N-2}(\mathbb{R}^N)]$, the exact sequence can be represented as follows:

$$\cdots \rightarrow \pi_2[\mathcal{O}(N)] \xrightarrow{i_1} \pi_2[V_{N-2}(\mathbb{R}^N)] \xrightarrow{i_2} \pi_1[\mathcal{O}(2)] \xrightarrow{i_3} \pi_1[\mathcal{O}(N)] \rightarrow \cdots . \quad (\text{S33})$$

From this sequence, we can deduce the following relationships:

$$\ker(i_2) = \text{im}(i_1) = 0, \quad \text{im}(i_2) = \ker(i_3) \cong 2\mathbb{Z}. \quad (\text{S34})$$

We utilize the fact that i_3 maps the even/odd numbers of \mathbb{Z} to 0/1 of \mathbb{Z}_2 , which leads to $\ker(i_3) \cong 2\mathbb{Z}$. Since $\pi_2[V_{N-2}(\mathbb{R}^N)]/\ker(i_2) \cong \text{im}(i_2)$, we can conclude that:

$$\pi_2[V_{N-2}(\mathbb{R}^N)] \cong 2\mathbb{Z}. \quad (\text{S35})$$

- For $\pi_2[V_M(\mathbb{R}^N)]$ with $M \leq N - 3$, the exact sequence is structured as follows:

$$\cdots \rightarrow \pi_2[\mathcal{O}(N)] \xrightarrow{i_1} \pi_2[V_M(\mathbb{R}^N)] \xrightarrow{i_2} \pi_1[\mathcal{O}(N - M)] \xrightarrow{i_3} \pi_1[\mathcal{O}(N)] \rightarrow \cdots . \quad (\text{S36})$$

Then, we know that

$$\ker(i_2) = \text{im}(i_1) = 0, \quad \text{im}(i_2) = \ker(i_3) = 0. \quad (\text{S37})$$

Here, we utilize the fact that i_3 is an isomorphism from \mathbb{Z}_2 to \mathbb{Z}_2 , which implies that $\ker(i_3) = 0$. Equation (S37) indicates that

$$\pi_2[V_M(\mathbb{R}^N)] = 0 \text{ for } M \leq N - 3. \quad (\text{S38})$$

- For $\pi_3[V_M(\mathbb{R}^N)]$ with $M \geq N - 2$, the exact sequence is structured as follows:

$$\cdots \rightarrow \pi_3[\mathrm{O}(N - M)] \xrightarrow{i_1} \pi_3[\mathrm{O}(N)] \xrightarrow{i_2} \pi_3[V_M(\mathbb{R}^N)] \xrightarrow{i_3} \pi_2[\mathrm{O}(N - M)] \xrightarrow{i_4} \pi_2[\mathrm{O}(N)] \rightarrow \cdots . \quad (\text{S39})$$

Then, we know that

$$\ker(i_3) = \mathrm{im}(i_2) = \mathbb{Z}/\ker(i_2) = \mathbb{Z}/\mathrm{im}(i_1) = \mathbb{Z}, \quad \mathrm{im}(i_3) = 0. \quad (\text{S40})$$

Since $\pi_3[V_M(\mathbb{R}^N)]/\ker(i_3) \cong \mathrm{im}(i_3)$, we obtain that

$$\pi_3[V_M(\mathbb{R}^N)] \cong \mathbb{Z} \text{ for } M \geq N - 2. \quad (\text{S41})$$

- For $\pi_3[V_{N-3}(\mathbb{R}^N)]$, the exact sequence is structured as follows:

$$\cdots \rightarrow \pi_3[\mathrm{O}(3)] \xrightarrow{i_1} \pi_3[\mathrm{O}(N)] \xrightarrow{i_2} \pi_3[V_{N-3}(\mathbb{R}^N)] \xrightarrow{i_3} \pi_2[\mathrm{O}(3)] \xrightarrow{i_4} \pi_2[\mathrm{O}(N)] \rightarrow \cdots . \quad (\text{S42})$$

Then, we know that

$$\ker(i_3) = \mathrm{im}(i_2) = \mathbb{Z}/\ker(i_2) = \mathbb{Z}/\mathrm{im}(i_1) \cong \mathbb{Z}_2, \quad \mathrm{im}(i_3) = 0. \quad (\text{S43})$$

Here, we utilize the fact that i_1 maps $2\mathbb{Z}$ to the even numbers of \mathbb{Z} , which implies that $\mathbb{Z}/\mathrm{im}(i_1) \cong \mathbb{Z}_2$. Since $\pi_3[V_{N-3}(\mathbb{R}^N)]/\ker(i_3) \cong \mathrm{im}(i_3)$, we obtain that

$$\pi_3[V_{N-3}(\mathbb{R}^N)] \cong \mathbb{Z}_2. \quad (\text{S44})$$

- For $\pi_3[V_M(\mathbb{R}^N)]$ with $M \leq N - 4$, the exact sequence is structured as follows:

$$\cdots \rightarrow \pi_3[\mathrm{O}(N - M)] \xrightarrow{i_1} \pi_3[\mathrm{O}(N)] \xrightarrow{i_2} \pi_3[V_M(\mathbb{R}^N)] \xrightarrow{i_3} \pi_2[\mathrm{O}(N - M)] \xrightarrow{i_4} \pi_2[\mathrm{O}(N)] \rightarrow \cdots . \quad (\text{S45})$$

Then, we know that

$$\ker(i_3) = \mathrm{im}(i_2) = \mathbb{Z}/\ker(i_2) = \mathbb{Z}/\mathrm{im}(i_1) = 0, \quad \mathrm{im}(i_3) = 0. \quad (\text{S46})$$

Here, we utilize the fact that i_1 is an isomorphism from \mathbb{Z} to \mathbb{Z} , which implies that $\mathbb{Z}/\mathrm{im}(i_1) = 0$. Then, we obtain that

$$\pi_3[V_M(\mathbb{R}^N)] = 0 \text{ for } M \leq N - 4. \quad (\text{S47})$$

3. Quaternionic Stiefel manifolds

As shown in Table I, we have $\pi_1[V_M(\mathbb{H}^N)] = 0$, $\pi_2[V_M(\mathbb{H}^N)] = 0$, and $\pi_3[V_M(\mathbb{H}^N)] = 0$. We will now present the derivation details that lead to these conclusions.

- For $\pi_1[V_M(\mathbb{H}^N)]$, the exact sequence is structured as follows:

$$\cdots \rightarrow \pi_1[\mathrm{Sp}_0(N)] \xrightarrow{i_1} \pi_1[V_M(\mathbb{H}^N)] \xrightarrow{i_2} \pi_0[\mathrm{Sp}_0(N - M)] \rightarrow \cdots . \quad (\text{S48})$$

From this, it follows that

$$\ker(i_2) = \mathrm{im}(i_1) = 0, \quad \mathrm{im}(i_2) = 0. \quad (\text{S49})$$

Hence, it can be deduced that

$$\pi_1[V_M(\mathbb{H}^N)] = 0. \quad (\text{S50})$$

- For $\pi_2[V_M(\mathbb{H}^N)]$, the exact sequence is structured as follows:

$$\cdots \rightarrow \pi_2[\mathrm{Sp}_0(N)] \xrightarrow{i_1} \pi_2[V_{N-1}(\mathbb{H}^N)] \xrightarrow{i_2} \pi_1[\mathrm{Sp}_0(N - M)] \rightarrow \cdots . \quad (\text{S51})$$

Based on this sequence, it can be established that

$$\ker(i_2) = \mathrm{im}(i_1) = 0, \quad \mathrm{im}(i_2) = 0. \quad (\text{S52})$$

The above equation indicates that

$$\pi_2[V_M(\mathbb{H}^N)] = 0. \quad (\text{S53})$$

- For $\pi_3[V_M(\mathbb{H}^N)]$, the exact sequence is structured as follows:

$$\cdots \rightarrow \pi_3[\mathrm{Sp}(N-M)_{\mathbb{Z}}] \xrightarrow{i_1} \pi_3[\mathrm{Sp}(N)_{\mathbb{Z}}] \xrightarrow{i_2} \pi_3[V_{N-1}(\mathbb{H}^N)] \xrightarrow{i_3} \pi_2[\mathrm{Sp}(N-M)_0] \rightarrow \cdots. \quad (\text{S54})$$

Based on this sequence, it can be inferred that

$$\ker(i_3) = \mathrm{im}(i_2) = \mathbb{Z}/\ker(i_2) = \mathbb{Z}/\mathrm{im}(i_1) = 0, \quad \mathrm{im}(i_3) = 0. \quad (\text{S55})$$

Here, we utilize the fact that i_1 is an isomorphism from \mathbb{Z} to \mathbb{Z} , which implies that $\mathbb{Z}/\mathrm{im}(i_1) = 0$. Equation (S55) indicates that

$$\pi_3[V_M(\mathbb{H}^N)] = 0. \quad (\text{S56})$$

II. Topological invariants

We will now give the methods for calculating the topological invariants for nontrivial topological classifications.

$$\mathbf{a.} \quad \pi_3[V_{N-1}(\mathbb{C}^N)] \cong \mathbb{Z}$$

Recalling Eq. (S21) and the fact that $\pi_3[V_{N-1}(\mathbb{C}^N)] \cong \mathbb{Z}$, we can obtain the following exact sequence:

$$\pi_3[\mathrm{U}(1)_0] \xrightarrow{i_1} \pi_3[\mathrm{U}(N)_{\mathbb{Z}}] \xrightarrow{i_2} \pi_3[V_{N-1}(\mathbb{C}^N)_{\mathbb{Z}}] \xrightarrow{i_3} \pi_2[\mathrm{U}(1)_0]. \quad (\text{S57})$$

As i_2 is an isomorphism from \mathbb{Z} to \mathbb{Z} , the topological invariant \mathcal{N} originates from $\pi_3[\mathrm{U}(N)] \cong \mathbb{Z}$. Since $\pi_2[\mathrm{U}(1)] = 0$, a globally well-defined $\mathcal{W}(\mathbf{k}) \in \mathrm{U}(N)$, given by Eq. (S6), exists throughout the Brillouin zone. Therefore, \mathcal{N} is simply the 3D winding number of the globally well-defined $\mathcal{W}(\mathbf{k})$, which is expressed as follows:

$$\mathcal{N} = \frac{1}{24\pi^2} \int_{\mathrm{BZ}} dk^3 \epsilon^{ijk} \mathrm{tr} \mathcal{W} \partial_i \mathcal{W}^\dagger \mathcal{W} \partial_j \mathcal{W}^\dagger \mathcal{W} \partial_k \mathcal{W}^\dagger \in \mathbb{Z}. \quad (\text{S58})$$

$$\mathbf{b.} \quad \pi_1[V_{N-1}(\mathbb{R}^N)] \cong \mathbb{Z}_2$$

Recalling Eq. (S24) and the fact that $\pi_1[V_{N-1}(\mathbb{R}^N)] \cong \mathbb{Z}_2$, we can obtain the following exact sequence:

$$\pi_1[\mathrm{O}(1)_0] \xrightarrow{i_1} \pi_1[\mathrm{O}(N)_{\mathbb{Z}_2}] \xrightarrow{i_2} \pi_1[V_{N-1}(\mathbb{R}^N)_{\mathbb{Z}_2}] \xrightarrow{i_3} \pi_0[\mathrm{O}(1)_{\mathbb{Z}_2}] \xrightarrow{i_4} \pi_0[\mathrm{O}(N)_{\mathbb{Z}_2}] \rightarrow \cdots. \quad (\text{S59})$$

As i_3 maps $\pi_1[V_{N-1}(\mathbb{R}^N)]$ to the trivial element of $\pi_1[\mathrm{O}(2)] \cong \mathbb{Z}_2$, i_2 is an isomorphism from \mathbb{Z}_2 to \mathbb{Z}_2 . Consequently, the topological invariant \mathcal{N} originates from $\pi_1[\mathrm{O}(N)] \cong \mathbb{Z}_2$. Since i_3 maps $\pi_1[V_{N-1}(\mathbb{R}^N)] \cong \mathbb{Z}_2$ to the trivial element of $\pi_0[\mathrm{O}(1)] \cong \mathbb{Z}_2$, there exists a globally well-defined $\mathcal{W}(k) \in \mathrm{O}(N)$, given by Eq. (S6), throughout the Brillouin zone. Therefore, \mathcal{N} is simply the homotopy invariant of the globally well-defined $\mathcal{W}(k)$. When $N = 2$, \mathcal{N} can be computed as

$$\mathcal{N} = \frac{1}{4\pi} \int_{T^1} dk \mathrm{tr} i\sigma_2 \mathcal{W} \partial_k \mathcal{W}^T \pmod{2}. \quad (\text{S60})$$

When $N > 2$, \mathcal{N} is equal to the parity of the number of times that the phases of the eigenvalues of $\mathcal{W}(k)$ cross π .

$$\mathbf{c.} \quad \pi_2[V_{N-2}(\mathbb{R}^N)] \cong 2\mathbb{Z}$$

Recalling Eq. (S33) and the fact that $\pi_2[V_{N-2}(\mathbb{R}^N)] \cong 2\mathbb{Z}$, we can obtain the following exact sequence:

$$\pi_2[\mathrm{O}(N)_0] \xrightarrow{i_1} \pi_2[V_{N-2}(\mathbb{R}^N)_{2\mathbb{Z}}] \xrightarrow{i_2} \pi_1[\mathrm{O}(2)_{\mathbb{Z}}] \xrightarrow{i_3} \pi_1[\mathrm{O}(N)_{\mathbb{Z}_2}] \xrightarrow{i_4} \pi_1[V_{N-2}(\mathbb{R}^N)_0]. \quad (\text{S61})$$

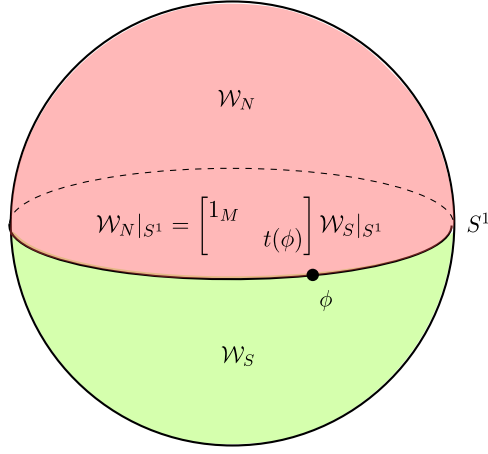


FIG. S1: A sphere S^2 is divided into two hemisphere D_N^2 and D_S^2 .

It is evident that i_2 maps $\pi_2[V_{N-2}(\mathbb{R}^N)] \cong 2\mathbb{Z}$ to the even numbers of $\pi_1[\text{O}(2)] \cong \mathbb{Z}$. Thus, the topological invariant \mathcal{N} actually originates from $\pi_1[\text{O}(2)] \cong \mathbb{Z}$.

Consider the 2D sphere S^2 in Fig. S1, which is divided into northern and southern hemispheres $D_{N/S}^2$ with their intersection at S^1 . We label $\mathcal{W}(\mathbf{k})$, given by Eq. (S6), as $\mathcal{W}_{N/S}$ on the hemisphere $D_{N/S}^2$. The transition function $t(\phi) \in \text{O}(2)$ glues $\mathcal{W}_{N/S}$ along the equator S^1 , as follows:

$$\mathcal{W}_N|_{S^1} = \begin{bmatrix} 1_{N-2} & \\ & t(\phi) \end{bmatrix} \mathcal{W}_S|_{S^1}. \quad (\text{S62})$$

Then, $\pi_1[\text{O}(2)] \cong \mathbb{Z}$ imposes obstructions to the globally well-defined $\mathcal{W}(\mathbf{k})$. Thus, we can calculate the topological invariant \mathcal{N} as the winding number of the transition function $t(\phi)$, that is,

$$\mathcal{N} = \frac{1}{4\pi} \int_{T^1} d\phi \text{tr} i\sigma_2 t \partial_\phi t^T \in 2\mathbb{Z}. \quad (\text{S63})$$

It is noteworthy that the winding number of $t(\phi)$ must be an even number. We can also compute the phase factors $\omega_{1/2}$ of the eigenvalues $\chi_{1,2}$ of $t(\phi)$. \mathcal{N} is equal to the number of times that ω_i crosses π .

$$\text{d. } \pi_3[V_{N-1}(\mathbb{R}^N)] \cong \mathbb{Z} \text{ and } \pi_3[V_{N-2}(\mathbb{R}^N)] \cong \mathbb{Z}$$

Recalling Eq. (S39) and the fact that $\pi_3[V_M(\mathbb{R}^N)] \cong \mathbb{Z}$ with $M \leq N - 2$, we obtain the following sequence:

$$\pi_3[\text{O}(N-M)_0] \xrightarrow{i_1} \pi_3[\text{O}(N)_\mathbb{Z}] \xrightarrow{i_2} \pi_3[V_M(\mathbb{R}^N)_\mathbb{Z}] \xrightarrow{i_3} \pi_2[\text{O}(N-M)_0]. \quad (\text{S64})$$

It is evident that i_2 is an isomorphism from \mathbb{Z} to \mathbb{Z} . Therefore, the topological invariant \mathcal{N} originates from $\pi_3[\text{O}(N)] \cong \mathbb{Z}$. Furthermore, since $\pi_2[\text{O}(N-M)] = 0$, a globally well-defined $\mathcal{W}(\mathbf{k}) \in \text{O}(N)$, which is defined in Equation (S6), always exists in the entire Brillouin zone. Consequently, \mathcal{N} is the 3D winding number of the globally well-defined $\mathcal{W}(\mathbf{k})$, which is given by:

$$\mathcal{N} = \frac{1}{48\pi^2} \int_{\text{BZ}} dk^3 \epsilon^{ijk} \text{tr} \mathcal{W} \partial_i \mathcal{W}^T \mathcal{W} \partial_j \mathcal{W}^T \mathcal{W} \partial_k \mathcal{W}^T \in \mathbb{Z}. \quad (\text{S65})$$

$$\text{e. } \pi_3[V_{N-3}(\mathbb{R}^N)] \cong \mathbb{Z}_2$$

Recalling Equation (S42) and the fact that $\pi_3[V_{N-3}(\mathbb{R}^N)] \cong \mathbb{Z}_2$, we obtain the following exact sequence:

$$\pi_4[V_{N-3}(\mathbb{R}^N)_0] \xrightarrow{i_1} \pi_3[\text{O}(3)_{2\mathbb{Z}}] \xrightarrow{i_2} \pi_3[\text{O}(N)_\mathbb{Z}] \xrightarrow{i_3} \pi_3[V_{N-3}(\mathbb{R}^N)_{\mathbb{Z}_2}] \xrightarrow{i_4} \pi_2[\text{O}(3)_0]. \quad (\text{S66})$$

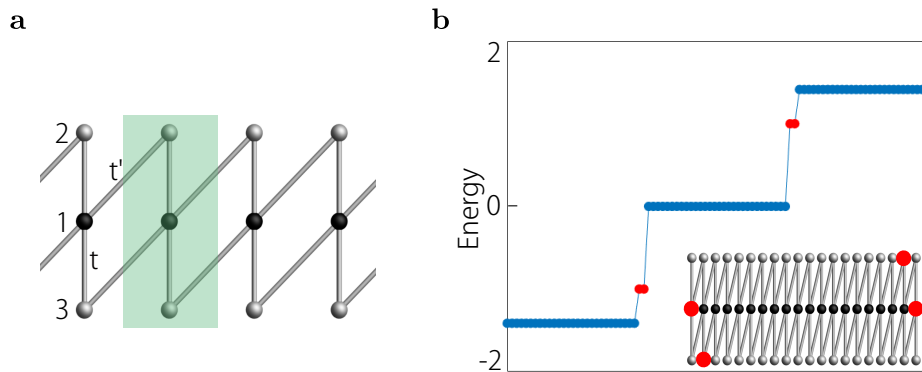


FIG. S2: **a** presents the one-dimensional lattice structure, wherein every unit cell accommodates three sites. The amplitudes of intracell and intercell hoppings are respectively denoted as t and t' . **b** shows four boundary states distributed on both ends with breaking the translational symmetry. The parameters are chosen as $t = 0$ and $t' = 1$.

In the above equation, since i_2 maps $\pi_3[\text{O}(3)] \cong 2\mathbb{Z}$ to the even numbers of $\pi_3[\text{O}(N)] \cong \mathbb{Z}$, i_3 maps even/odd numbers of \mathbb{Z} to the trivial/nontrivial element of $\pi_3[\text{O}(N)] \cong \mathbb{Z}$. Additionally, since $\pi_2[\text{O}(3)] = 0$, a globally well-defined $\mathcal{W}(\mathbf{k}) \in \text{O}(N)$, as given in Equation (S6), always exists in the entire Brillouin zone. Consequently, the topological invariant \mathcal{N} is the parity of the 3D winding number of the globally well-defined $\mathcal{W}(\mathbf{k}) \in \text{O}(N)$, expressed as:

$$\mathcal{N} = \frac{1}{48\pi^2} \int_{\text{BZ}} dk^3 \epsilon^{ijk} \text{tr} \mathcal{W} \partial_i \mathcal{W}^T \mathcal{W} \partial_j \mathcal{W}^T \mathcal{W} \partial_k \mathcal{W}^T \pmod{2}. \quad (\text{S67})$$

The reduction of the invariant from \mathbb{Z} to \mathbb{Z}_2 is due to the requirement that a topological invariant for \mathcal{W} should remain unchanged under any gauge transformation (S7). Through straightforward derivations, it can be shown that:

$$\mathcal{N}[\mathcal{W}'] = \mathcal{N}[\mathcal{W}] + \mathcal{N}[\mathcal{G}] \quad (\text{S68})$$

where $\mathcal{W}' = \text{diag}[1_M, \mathcal{G}]\mathcal{W}$ and $\mathcal{G} \in \text{O}(3)$. When substituting a topologically nontrivial \mathcal{G} into the formula (S67), an even integer $\nu[\mathcal{G}] \in 2\mathbb{Z}$ is obtained, which is consistent with $\pi_3[\text{O}(N)] \cong 2\mathbb{Z}$. Therefore, only the parity of the integer is meaningful here, justifying the \mathbb{Z}_2 nature of the topological invariant (S67).

III. Matrix representation of spin-1 operators

The matrices $S_{x,y,z}$ in the manuscript are given by

$$S_x = \frac{1}{\sqrt{2}} \begin{bmatrix} 0 & 1 & 1 \\ 1 & 0 & 0 \\ 1 & 0 & 0 \end{bmatrix}, \quad S_y = \frac{1}{\sqrt{2}} \begin{bmatrix} 0 & -i & i \\ i & 0 & 0 \\ -i & 0 & 0 \end{bmatrix}, \quad S_z = \frac{1}{\sqrt{2}} \begin{bmatrix} 0 & 0 & 0 \\ 0 & -1 & 0 \\ 0 & 0 & 1 \end{bmatrix}, \quad (\text{S69})$$

satisfying that

$$[S_i, S_j] = i\epsilon_{ijk} S_k. \quad (\text{S70})$$

IV. A 1D insulator model with CSNES and \mathcal{PT} symmetry

As shown in Fig. S2(a), we present a one-dimensional model corresponding to the classifying space $V_{N-1}(\mathbb{R}^N)$. Each unit cell consists of one A -site and two B -sites, indicated by black and grey coloring respectively. This model only incorporates hoppings between different sublattices, indicating the presence of sublattice symmetry \mathcal{S} . The intracell and intercell hopping amplitudes are denoted as t and t' , respectively. Since all hoppings are real, the time reversal symmetry \mathcal{T} is preserved. Furthermore, this model exhibits inversion symmetry through the center of the unit cell.

The inversion symmetry \mathcal{P} preserves the sublattices, leading to its commutation with \mathcal{S} . The combined symmetry \mathcal{PT} also commutes with \mathcal{S} . In momentum space, the Hamiltonian is given by

$$\mathcal{H}_{1D}(k) = \begin{bmatrix} 0 & w(k) & w^*(k) \\ w^*(k) & 0 & 0 \\ w(k) & 0 & 0 \end{bmatrix}, \quad (\text{S71})$$

where $w_{\pm}(k) = t + t'e^{-ik}$. The symmetry operators are represented as $\mathcal{S} = \text{diag}[1, -1_2]$ and $\mathcal{PT} = \text{diag}[1, \sigma_1]\mathcal{K}$. The energy spectrum of this Hamiltonian features eigenvalues of 0 and $\pm\sqrt{2}|w(k)|$. Notably, when $t = \pm t'$, two bulk gaps close.

To obtain the real Hamiltonian, we apply a unitary transformation $U = 1 \oplus e^{-i\pi/4}e^{i\pi\sigma_1/4}$ to this system. \mathcal{PT} symmetry is transformed as $U\mathcal{PT}U^\dagger = \hat{\mathcal{K}}$, while \mathcal{S} is preserved. The resulting real Hamiltonian $\mathcal{H}_{1D}^{\mathbb{R}}(k) = U\mathcal{H}_{1D}(k)U^\dagger$ is given by

$$\mathcal{H}_{1D}^{\mathbb{R}}(k) = \begin{bmatrix} 0 & w_+(k) & w_-(k) \\ w_+(k) & 0 & 0 \\ w_-(k) & 0 & 0 \end{bmatrix}, \quad (\text{S72})$$

where $w_{\pm}(k) = t + t'(\cos k \pm \sin k)$. For the 1D model (S71), the expression of $\mathcal{W}(k)$ defined in Eq. (S6) is given by

$$\mathcal{W}(k) = (w_+(k)\sigma_3 + w_-(k)\sigma_1)/E(k). \quad (\text{S73})$$

Substituting this $\mathcal{W}(k)$ into Eq. (S60), we find that $\nu = 1$ when $|t| < |t'|$ and $\nu = 0$ when $|t| > |t'|$. As depicted in Fig. S2(b), if we break the translational symmetry and set the parameters as $t = 0$ and $t' = 1$, two pairs of inversion-related in-gap states emerge on the ends.

V. The Ten-band PZSV lattice model with CSNES and $C_{2z}\mathcal{T}$ symmetry

a. Euler class of the flat bands

Before presenting the model, we will first prove that the topological invariant \mathcal{N} in Eq. (S63) is actually the Euler class of the two flat bands in the bulk band structure. The corresponding system should possess chiral symmetry with $\hat{\mathcal{S}} = \text{diag}\{1_{N-2}, 1_N\}$, and \mathcal{PT} symmetry with $(\mathcal{PT})^2 = 1$ and $[\mathcal{S}, \mathcal{PT}] = 0$. The existence of two flat bands in the bulk band structure is a consequence of the form of \mathcal{S} . The homotopy group is given by $\pi_2[V_{N-2}(\mathbb{R}^N)] \cong 2\mathbb{Z}$.

Since \mathcal{PT} symmetry makes $\mathcal{U}(\mathbf{k})$ in Eq. (S3) be a real orthogonal matrix, we can express $\mathcal{U}(\mathbf{k})$ as

$$\mathcal{U}(\mathbf{k}) = (|\psi_1(\mathbf{k})\rangle, |\psi_2(\mathbf{k})\rangle, \dots, |\psi_{N-1}(\mathbf{k})\rangle, |\psi_N(\mathbf{k})\rangle), \quad (\text{S74})$$

where $|\psi_i(\mathbf{k})\rangle$ are real column vectors. From Eq. (S4), we know that

$$\mathcal{H}(\mathbf{k})|\varphi_i(\mathbf{k})\rangle = 0, \quad |\varphi_i(\mathbf{k})\rangle = \begin{bmatrix} 0_{(N-2)\times 1} \\ |\psi_{N+i-2}(\mathbf{k})\rangle \end{bmatrix}, \quad (\text{S75})$$

with $i = 1$ and 2 . In other words, $|\varphi_{1,2}(\mathbf{k})\rangle$ correspond to the eigenvectors of the two flat bands. Referring to Fig. S1 and Eq. (S62), the transition function $t(\phi)$ defined on the equator S^1 satisfies

$$\begin{bmatrix} 1_{N-2} & \\ & t(\phi) \end{bmatrix} = \mathcal{W}_N|_{S^1} \mathcal{W}_S^T|_{S^1} = \begin{bmatrix} \mathcal{V}_N|_{S^1} & \\ & 1_2 \end{bmatrix} \mathcal{U}_N^T|_{S^1} \mathcal{U}_S|_{S^1} \begin{bmatrix} \mathcal{V}_S^T|_{S^1} & \\ & 1_2 \end{bmatrix} = \mathcal{U}_N^T|_{S^1} \mathcal{U}_S|_{S^1}. \quad (\text{S76})$$

Let us label the flat band eigenvectors on the semisphere $D_{N/S}^2$ as $|\varphi_i^{N/S}\rangle$. Substituting Eq. (S74) and Eq. (S75) into Eq. (S76), the matrix element of the 2×2 matrix $t(\phi)$ is given by

$$t_{ij}(\phi) = \langle \varphi_i^N(\phi) | \varphi_j^S(\phi) \rangle. \quad (\text{S77})$$

The above equation shows that the transition function $t(\phi)$ of $\mathcal{W}(\mathbf{k})$ is also the transition function of the eigenvectors of the flat bands. Moreover, we can apply the Wilson loop method to the flat bands, and the Wilson loop operator has the same eigenvalues as $t(\phi)$. From the definition of the Euler class, we know that the winding number \mathcal{N} in Eq. (S63) corresponds to the Euler class of the two flat bands. Thus, the topological invariant \mathcal{N} is equal to the number of times that the Wilson loop spectra crosses π .

b. The PZSV model

Near the first magic angle ($\theta \approx 1.05^\circ$), twisted bilayer graphene (TBG) exhibits two almost perfectly flat bands for each spin and valley degree of freedom. In this work, we adopt the ten-band Po-Zou-Senthil-Vishwanath (PZSV) tight-binding model proposed by Vishwanath to capture the low-energy physics of single-valley TBG (See Ref. [12] in the main text). This model preserves both the CSNES and $C_{2z}\mathcal{T}$ symmetry. In two dimensions, $C_{2z}\mathcal{T}$ symmetry imposes the same constraints on $\mathcal{H}(\mathbf{k})$ as \mathcal{PT} symmetry. And the two nearly flat bands in the bulk band structure of TBG arise from the CSNES.

The lattice structure of the PZSV model is illustrated in Fig. S3(a), where each unit cell contains ten orbitals: a_i^\dagger with i ranging from 1 to 4 for A -sites, and b_j^\dagger with j ranging from 1 to 6 for B -sites. The specific orbital content of each sublattice is shown in the top-right inset of Fig. S3(a). The hopping terms only exist between a_i^\dagger and b_j^\dagger , and thus the chiral symmetry can be expressed as

$$\hat{S} = \begin{bmatrix} 1_4 & \\ & -1_6 \end{bmatrix}. \quad (\text{S78})$$

The PZSV model is invariant under $C_{2z}\mathcal{T}$ symmetry with the inversion center located at the blue dot labeled by b_1^\dagger in Fig. S3(a). Under the $C_{2z}\mathcal{T}$ operation, s -orbitals and p_z -orbitals remain invariant, while the p_+ -orbitals and p_- -orbitals are exchanged. Therefore, the $C_{2z}\mathcal{T}$ symmetry is given by

$$\hat{C}_{2z}\hat{\mathcal{T}} = \begin{bmatrix} 0 & 0 & 0 & 1 & 0 & 0 & 0 & 0 & 0 & 0 \\ 0 & 0 & 1 & 0 & 0 & 0 & 0 & 0 & 0 & 0 \\ 0 & 1 & 0 & 0 & 0 & 0 & 0 & 0 & 0 & 0 \\ 1 & 0 & 0 & 0 & 0 & 0 & 0 & 0 & 0 & 0 \\ 0 & 0 & 0 & 0 & 1 & 0 & 0 & 0 & 0 & 0 \\ 0 & 0 & 0 & 0 & 0 & 0 & 1 & 0 & 0 & 0 \\ 0 & 0 & 0 & 0 & 0 & 1 & 0 & 0 & 0 & 0 \\ 0 & 0 & 0 & 0 & 0 & 0 & 0 & 1 & 0 & 0 \\ 0 & 0 & 0 & 0 & 0 & 0 & 0 & 0 & 1 & 0 \\ 0 & 0 & 0 & 0 & 0 & 0 & 0 & 0 & 0 & 1 \end{bmatrix} \hat{\mathcal{K}}. \quad (\text{S79})$$

Since $\hat{S} = \text{diag}\{1_4, -1_6\}$, $(C_{2z}\mathcal{T})^2 = 1$, and $[\mathcal{S}, C_{2z}\mathcal{T}] = 0$, the PZSV model is classified into the real Stiefel manifold $V_4(\mathbb{R}^6)$. The Bravais lattice vectors of the PZSV lattice are chosen as

$$\mathbf{a}_1 = (\sqrt{3}/2, -1/2, 0), \quad \mathbf{a}_2 = (0, 1, 0), \quad \mathbf{a}_3 = (0, 0, 1). \quad (\text{S80})$$

The translation along the z -direction is only considered for calculating the reciprocal lattice vectors $\mathbf{b}_{1,2}$, which are given by

$$\mathbf{b}_1 = \frac{\mathbf{a}_2 \times \mathbf{a}_3}{\mathbf{a}_1 \cdot (\mathbf{a}_2 \times \mathbf{a}_3)} = \left(\frac{2}{\sqrt{3}}, 0, 0\right), \quad \mathbf{b}_2 = \frac{\mathbf{a}_3 \times \mathbf{a}_1}{\mathbf{a}_2 \cdot (\mathbf{a}_3 \times \mathbf{a}_1)} = \left(\frac{1}{\sqrt{3}}, 1, 0\right). \quad (\text{S81})$$

Then, in the momentum space, the Fourier-transformed operators are given by

$$a_{\mathbf{k},i}^\dagger = \frac{1}{\sqrt{N}} \sum_{\mathbf{R}} a_{\mathbf{R},i}^\dagger e^{-i\mathbf{k} \cdot (\mathbf{R} + \mathbf{r}_i^a)}, \quad b_{\mathbf{k},j}^\dagger = \frac{1}{\sqrt{N}} \sum_{\mathbf{R}} b_{\mathbf{R},j}^\dagger e^{-i\mathbf{k} \cdot (\mathbf{R} + \mathbf{r}_j^b)}, \quad (\text{S82})$$

where \mathbf{R} labels the unit cell, $\mathbf{r}_i^{a/b}$ denotes the displacement of the $a_{\mathbf{R},i}^\dagger$ fermion relative to the unit cell origin, and $\mathbf{k} = k_1\mathbf{b}_1 + k_2\mathbf{b}_2$ represents the crystalline momentum. Thus, the Bloch Hamiltonian is given by

$$H(\mathbf{k}) = \sum_{\mathbf{k}} \Psi^\dagger(\mathbf{k}) \mathcal{H}(\mathbf{k}) \Psi(\mathbf{k}), \quad (\text{S83})$$

with the momentum space spinor

$$\Psi^\dagger(\mathbf{k}) = (a_{\mathbf{k},1}^\dagger, \dots, a_{\mathbf{k},4}^\dagger, b_{\mathbf{k},1}^\dagger, \dots, b_{\mathbf{k},6}^\dagger), \quad (\text{S84})$$

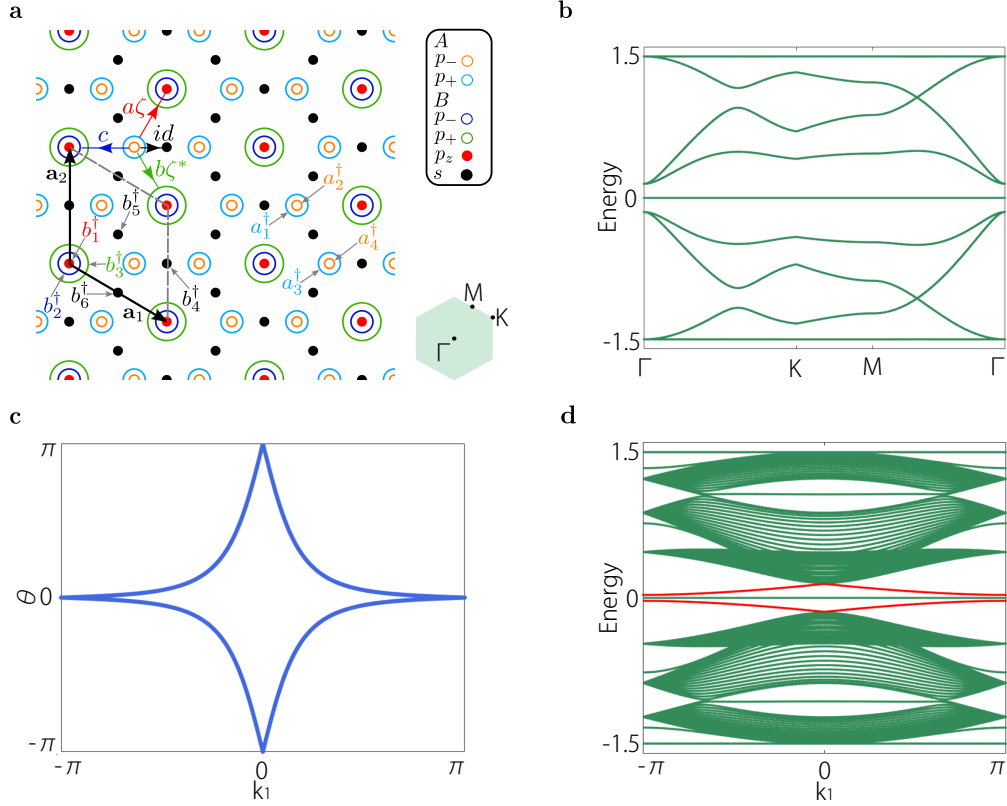


FIG. S3: **a** illustrates the lattice structure of the ten-band PZSV lattice model. The unit cell, represented by a dashed gray square, consists of 10 orbitals. As detailed in the inset at the top-right of the panel, A -sublattice contains two p_- -orbitals and two p_+ -orbitals, whereas B -sublattice contains one p_- -orbital, one p_+ -orbital, one p_z -orbital and three s -orbitals. Here, we use the convention of Ref. [12] in the main text, where $p_{\pm} = \frac{1}{\sqrt{2}}(p_x \pm ip_y)$. The first Brillouin zone is shown in the bottom-right inset. In **b**, **c** and **d**, the hopping parameters are set as $a = 0.110$, $b = 0.033$, $c = 0.033$, and $d = 0.573$. **b** displays the bulk band structure of the PZSV model, where two flat bands exist because of the form of CSNES. **c** shows the Wilson loop spectra of the flat bands along the circles C_{k_1} (k_1 is fixed for each circle) parameterized by k_2 . **d** shows the edge states when the boundary along \mathbf{a}_1 is opened.

and the first-quantized Hamiltonian

$$\mathcal{H}(\mathbf{k}) = \begin{bmatrix} & \mathcal{Q}(\mathbf{k}) \\ \mathcal{Q}^\dagger(\mathbf{k}) & \end{bmatrix}. \quad (\text{S85})$$

Here, the elements of the 4×6 matrix $\mathcal{Q}(\mathbf{k})$ are obtained through the Fourier transformation

$$[\mathcal{Q}(\mathbf{k})]_{ij} = \sum_{\mathbf{R}} [\mathcal{Q}_{\mathbf{R}}]_{ij} e^{i\mathbf{k} \cdot (\mathbf{R} + \mathbf{r}_i^a - \mathbf{r}_j^b)}, \quad (\text{S86})$$

where $\mathcal{Q}_{\mathbf{R}}$ represents the inter-sublattice hopping matrix. The i -th column of the 4×6 matrix $\mathcal{Q}(\mathbf{k})$, denoted by $\mathcal{Q}_{:,i}(\mathbf{k})$, can be expressed as

$$\mathcal{Q}_{:,1} = \begin{bmatrix} -a\zeta e^{i(k_1+2k_2)/3} (\eta e^{-i(k_1+k_2)} + e^{-ik_2} + \eta^*) \\ a\zeta e^{i(k_1+2k_2)/3} (\eta e^{-i(k_1+k_2)} + \eta^* e^{-ik_2} + 1) \\ a\zeta^* e^{i(2k_1+k_2)/3} (e^{-i(k_1+k_2)} + \eta e^{-ik_1} + \eta^*) \\ -a\zeta^* e^{i(4k_1+5k_2)/6} (\eta e^{-i(k_1+3k_2/2)} + e^{-i(k_1+k_2/2)} + \eta^* e^{-ik_2/2}) \end{bmatrix}, \quad (\text{S87})$$

$$\mathcal{Q}_{:,2} = \begin{bmatrix} b\zeta^* e^{i(k_1+2k_2)/3} (\eta + \eta^* e^{-i(k_1+k_2)} + e^{-ik_2}) \\ c e^{i(k_1+2k_2)/3} (e^{-i(k_1+k_2)} + e^{-ik_2} + 1) \\ b\zeta e^{i(4k_1+5k_2)/6} (e^{-i(k_1+3k_2/2)} + \eta^* e^{-i(k_1+k_2/2)} + \eta e^{-ik_2/2}) \\ c (e^{-i(k_1+2k_2)/3} + e^{i(-k_1+k_2)/3} + e^{i(2k_1+k_2)/3}) \end{bmatrix}, \quad (\text{S88})$$

$$\mathcal{Q}_{:,3} = \begin{bmatrix} ce^{i(k_1+2k_2)/3}(e^{-i(k_1+k_2)} + e^{-ik_2} + 1) \\ b\zeta^* e^{i(k_1+2k_2)/3}(1 + \eta^* e^{-i(k_1+k_2)} + \eta e^{-ik_2}) \\ c(e^{-i(k_1+2k_2)/3} + e^{i(-k_1+k_2)/3} + e^{i(2k_1+k_2)/3}) \\ b\zeta e^{i(4k_1+5k_2)/6}(\eta^* e^{-i(k_1+3k_2/2)} + e^{-i(k_1+k_2/2)} + \eta e^{-ik_2/2}) \end{bmatrix}, \quad (\text{S89})$$

$$\mathcal{Q}_{:,4} = \begin{bmatrix} ide^{i(2k_1+k_2)/6} \\ ide^{i(2k_1+k_2)/6} \\ -ide^{-i(2k_1+k_2)/6} \\ -ide^{-i(2k_1+k_2)/6} \end{bmatrix}, \quad \mathcal{Q}_{:,5} = \begin{bmatrix} id\eta^* e^{i(-k_1+k_2)/6} \\ id\eta e^{i(-k_1+k_2)/6} \\ -id\eta^* e^{i(k_1-k_2)/6} \\ -id\eta e^{i(k_1-k_2)/6} \end{bmatrix}, \quad \mathcal{Q}_{:,6} = \begin{bmatrix} id\eta e^{-i(k_1+2k_2)/6} \\ id\eta^* e^{-i(k_1+2k_2)/6} \\ id\eta e^{i(k_1+2k_2)/6} \\ id\eta^* e^{i(k_1+2k_2)/6} \end{bmatrix}. \quad (\text{S90})$$

Here, a , b , c , and d are hopping parameters, while $\zeta = e^{i\pi/3}$ and $\eta = \zeta^2$ are fixed values.

In the first Brillouin zone $(k_1, k_2) \in [-\pi, \pi]^2$, the Hamiltonian $\mathcal{H}(\mathbf{k})$ is non-periodic. However, we can consider the periodic Hamiltonian $\mathcal{H}'(\mathbf{k}) = V(\mathbf{k})\mathcal{H}(\mathbf{k})V^\dagger(\mathbf{k})$, where $V(\mathbf{k})$ is given by

$$V(\mathbf{k}) = \begin{bmatrix} e^{2i(k_1-k_2)/3} & 0 & 0 & 0 & 0 & 0 & 0 & 0 & 0 & 0 \\ 0 & e^{2i(k_1-k_2)/3} & 0 & 0 & 0 & 0 & 0 & 0 & 0 & 0 \\ 0 & 0 & e^{i(k_1-k_2)/3} & 0 & 0 & 0 & 0 & 0 & 0 & 0 \\ 0 & 0 & 0 & e^{i(k_1-k_2)/3} & 0 & 0 & 0 & 0 & 0 & 0 \\ 0 & 0 & 0 & 0 & 1 & 0 & 0 & 0 & 0 & 0 \\ 0 & 0 & 0 & 0 & 0 & 1 & 0 & 0 & 0 & 0 \\ 0 & 0 & 0 & 0 & 0 & 0 & 1 & 0 & 0 & 0 \\ 0 & 0 & 0 & 0 & 0 & 0 & 0 & e^{-ik_2/2} & 0 & 0 \\ 0 & 0 & 0 & 0 & 0 & 0 & 0 & 0 & e^{i(k_1-k_2)/2} & 0 \\ 0 & 0 & 0 & 0 & 0 & 0 & 0 & 0 & 0 & e^{ik_1/2} \end{bmatrix}. \quad (\text{S91})$$

The matrix element of $V(\mathbf{k})$ is obtained as $[V(\mathbf{k})]_{ij} = \delta_{ij} e^{i\mathbf{k}\cdot\mathbf{r}_i}$, where \mathbf{r}_i denotes the displacement of the $a_{\mathbf{R},i}^\dagger$ ($b_{\mathbf{R},i-4}^\dagger$) fermion relative to the unit cell origin for $1 \leq i \leq 4$ ($5 \leq i \leq 10$).

For a reciprocal lattice translation $\mathbf{K} = 2\pi(m\mathbf{b}_1 + n\mathbf{b}_2)$ with $m, n \in \mathbb{Z}$, we have

$$\mathcal{H}(\mathbf{k} + \mathbf{K}) = V^\dagger(\mathbf{K})\mathcal{H}(\mathbf{k})V(\mathbf{K}). \quad (\text{S92})$$

Thus, given the eigenvectors $|\psi_i(\mathbf{k})\rangle$ of $\mathcal{H}(\mathbf{k})$, $V^\dagger(\mathbf{K})|\psi_i(\mathbf{k})\rangle$ should be the eigenvectors of $\mathcal{H}(\mathbf{k} + \mathbf{K})$. Now, to elaborate the Wilson loop calculation for the non-periodic Hamiltonian $\mathcal{H}(\mathbf{k})$ in Eq. (S85), we consider the 1D insulator subsystem and divide the 1D first Brillouin zone into N intervals labeled by separation points $i = 0, 1, \dots, N$. The Wilson loop operator $W^{(\Lambda)}$ is then expressed as

$$W^{(\Lambda)} = \lim_{N \rightarrow \infty} \left(\prod_{i=0}^{N-2} F_{(i,i+1)} \right) \times F_{(N-1,N)}^{(\Lambda)}, \quad (\text{S93})$$

with

$$[F_{(i,i+1)}]_{ab} = \langle a, k_{(i)} | b, k_{(i+1)} \rangle, \quad [F_{(N-1,N)}^{(\Lambda)}]_{ab} = \langle a, k_{(N-1)} | \Lambda | b, k_{(0)} \rangle. \quad (\text{S94})$$

Here, the indices a and b label the bands, and $\Lambda = V^\dagger(2\pi\mathbf{b}_{1,2})$ is used when calculating the Wilson loop along the circles $C_{k_{2,1}}$ (with $k_{2,1}$ fixed for each circle) parameterized by $k_{1,2}$, respectively.

In Vishvanath's paper, the PZSV model is characterized by four hopping parameters: $a = 0.110$, $b = 0.033$, $c = 0.033$, and $d = 0.573$ (in dimensionless units). Under this parameter condition, the bulk band structure is shown in Fig. S3(b). The form of \mathcal{S} induces two flat bands. The Wilson loop spectra of the two flat bands are displayed in Fig. S3(c), revealing an Euler class of 1. Therefore, the topological invariant defined in Eq. (S63) is $\mathcal{N} = 1$. Notably, \mathcal{N} is not an even number due to the non-periodicity of $\mathcal{H}(\mathbf{k})$. If we consider the Hamiltonian (S85) within the extended period $(k_1, k_2) \in [-6\pi, 6\pi]^2$, \mathcal{N} would be the even number 36. The edge states with opening the boundary along \mathbf{a}_1 are shown in Fig. S3(d).